lower layer adjacent to the surface has a uniform basic wind and serves as a wave duct when the conditions are met. They showed that when the shear layer is dynamically stable (Ri≥1/4), almost all of the wave energy is absorbed near the critical level. However, when the shear layer is dynamically unstable, waves can be partially- or over-reflected from the critical level depending upon the strength of the stability of the shear layer. The wave is almost entirely reflected when $(Ri-1/4)^{1/2}$ is near 0.4. The transmission coefficient increases as the reflection coefficient increases. In addition, the wave amplitude below the shear layer also depends upon the depth of the lower layer of uniform flow. The wave amplitude in the lower layer becomes maximum when the ratio of the vertical wavelength and the depth of the lower layer is n/2+1/4. These factors may modify the vertical motion field significantly, which in turn will either enhance or suppress the new cells produced by the density current.

5.2 Three-Dimensional Flow

a. Uniform flow

Before we discuss the response of a three-dimensional shear flow to elevated heating, it is essential to understand the response of a three-dimensional uniform flow to an elevated heating. Thus, we will review the work of Lin (1986a) first and then the work of Lin and Li (1988). The small-amplitude equation governing the vertical velocity for a steady state, three-dimensional, stratified, incompressible, Boussinesq, non-rotating flow can be written

$$(U\frac{\partial}{\partial x}+\nu)^2\nabla^2 w' + N^2\nabla_H^2 w' = (\frac{g}{c_pT_o})\nabla_H^2 q' \qquad (5.15)$$

where ν is the coefficient of both Rayleigh friction and Newtonian cooling. To solve the above equation, we determine the relevant Green's function as in previous sections. Taking the double Fourier transform in x and y (x --> k, y --> l) of the above equation, we have

$$\hat{w}_{zz}+\frac{[N^2-(Uk-i\nu)^2]K^2}{(Uk-i\nu)^2}\hat{w}=\frac{gK^2}{c_pT_o(Uk-i\nu)^2}\hat{q}, \qquad (5.16)$$

where $K=(k^2+l^2)^{1/2}$ is the horizontal wave number.

Consider a bell-shaped heat source with circular contours

$$q'(x,y,z)=\frac{Q_o}{(r^2/b^2+1)^{3/2}}\delta(z), \qquad (5.17)$$

where

$$r=(x^2+y^2)^{1/2}.$$

Taking the double Fourier transform of the above equation and substituting into Eq. (5.16), we obtain

$$\hat{w}_{zz}+\lambda^2\hat{w}=\frac{gQ_ob^2K^2e^{-bK}}{2\pi c_pT_o(Uk-i\nu)^2}\delta(z), \qquad z\geq -H \qquad (5.18)$$

where

$$\lambda^2=\frac{[N^2-(Uk-i\nu)^2]K^2}{(Uk-i\nu)^2} \qquad (5.19)$$

An approximate set of lower and upper boundary conditions are $\hat{w}=0$ at the surface (z=-H) and the radiation condition, i.e. $\hat{w}\sim\exp(i\lambda z)$ as z --> ∞. At the interface z=0, one condition is that $\hat{w}$ is continuous across the interface. Integrating Eq. (5.18) across the interface yields another condition that $\hat{w}_z$ is continuous. Thus the solution of Eq. (5.18) can be obtained

$$\hat{w}(k, l, z) = \frac{igQ_o b^2 K e^{-bK}[e^{i\lambda(z+2H)} - e^{i\lambda|z|}]}{4\pi c_p T_o (Uk-iv)\,[N^2-(Uk-iv)^2]^{1/2}} \tag{5.20}$$

The vertical displacement, η, defined by $w=U\partial\eta/\partial x$, may be written as

$$\eta(x,y,z) = \iint_{-\infty}^{\infty} \frac{gQ_o b^2\, K e^{-bK}\,[e^{i\lambda(z+2H)} - e^{i\lambda|z|}]}{4\pi c_p T_o U k(Uk-iv)\sqrt{N^2-(Uk-iv)^2}} \cdot e^{i(kx+ly)}\,dk\,dl \qquad z \geq -H. \tag{5.21}$$

The above equation may be nondimensionalized by

$$(\tilde{x}, \tilde{y}) = (x/b, y/b);\ (\tilde{k}, \tilde{l}, \tilde{K}) = (bk, bl, bK);$$
$$\tilde{v} = vb/U;(\tilde{\eta}, \tilde{z}, \tilde{H}) = (\eta N/U, zN/U, HN/U);$$
$$\tilde{Q_o} = Q_o gb/(c_p T_o U^3) \tag{5.22}$$

to yield

$$\eta(x,y,z) = \iint_{-\infty}^{\infty} \frac{\hat{q}(K)\,K\,[e^{i\lambda(z+2H)} - e^{i\lambda|z|}]}{2k(k-iv)\sqrt{1-M^2(k-iv)^2}} \cdot e^{i(kx+ly)}\,dk\,dl, \tag{5.23}$$

where

$$\hat{q}(K) = \frac{Q_o}{2\pi} e^{-K}.$$

Notice that the nonhydrostatic effect is represented by a nondimensional number M (=U/bN), which is proportional to the ratio of the period of a buoyancy oscillation (2π/N) to the time it takes for an air parcel to pass the heat source (b/U). This reasoning is similar to the mountain wave problem in which the horizontal scale is measured by the mountain width. For simplicity, we assume the flow is hydrostatic (M<<1) in most cases. A two-dimensional FFT (Fast Fourier Transform, see Smith, 1979 for a brief review) algorithm can be employed to invert the above solution back to the physical space.

Fig. 36 shows an example of a hydrostatic flow

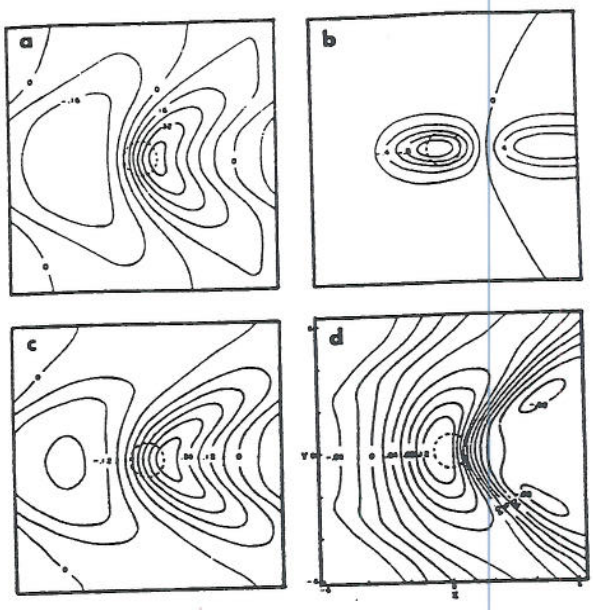

Fig. 36: Vertical displacement of a three-dimensional, continuously stratified, hydrostatic, uniform flow over an isolated heat source which is added at z=0. The dashed circle is the heating contour at r=b. The basic flow is directed from left to right in the positive x direction. The solution is given by Eq. (5.23) with $H=\pi$, M=0, v=0.2. The four levels shown are: (a) $-\pi/2$, (b) 0, (c) $\pi/2$, and (d) π. (From Lin, 1986a)

(M=0) over a shallow heat source with $\tilde{H}=\pi$. The dimensional parameters may be considered as U=10 m s^{-1}, N=0.01 s^{-1}, b=5 km, and H=3.14 km. The response of the fluid to the heating at the heating level (z=0) is a downward displacement upstream of the prescribed heat source followed by an upward displacement downstream. This is similar to the two-dimensional flow as studied in earlier sections. The region of disturbance widens in general as one moves aloft and beneath the heating level. A V-shaped pattern in the region of upward displacement

forms above the heating center at the level of $z=\pi/2$. This region of upward displacement is shifted upstream as one moves further aloft as required by the upper radiation condition. At the level of $z=\pi$, a new region of downward displacement forms just downstream of the V-shaped area of upward displacement. The response is almost periodic in the vertical with a wavelength of π (e.g., comparing Fig. 36a,c) like that in the hydrostatic mountain waves (Queney, 1947; Smith, 1979). The amplitude of the vertical displacement decreases vertically, which is mainly due to the divergence above the heating region and the viscosity.

The vertical cross section at y=0 for the above case is plotted in Fig. 37a. The upstream phase tilt of the disturbance above the heating level (z=0) indicates that the wave energy is able to propagate upward (Eliassen and Palm, 1960). The term $\exp(i\lambda(z+2H))$ in the numerator of Eq. (5.23) represents the reflected waves from the surface, which may cancel the direct upgoing wave, i.e., the term $\exp(i\lambda|z|)$, above the heating level with certain values of H. This is similar to the two-dimensional flow (Smith and Lin, 1982). One example with $H=2\pi$ is shown in Fig. 37b in which the disturbance above the heating level (z=0) is much weaker than the case of Fig. 37a.

The formation of the V-shaped pattern of the vertical displacement can be explained by the group velocity argument (Lin and Li, 1988). The dispersion relation for an internal gravity waves in a stagnant Boussinesq fluid is

$$\omega = \pm \left[\frac{N^2(k^2+l^2)}{k^2+l^2+m^2}\right]^{1/2}, \tag{5.24}$$

where ω and m are the frequency and the vertical wave number, respectively. The group velocity can then be found:

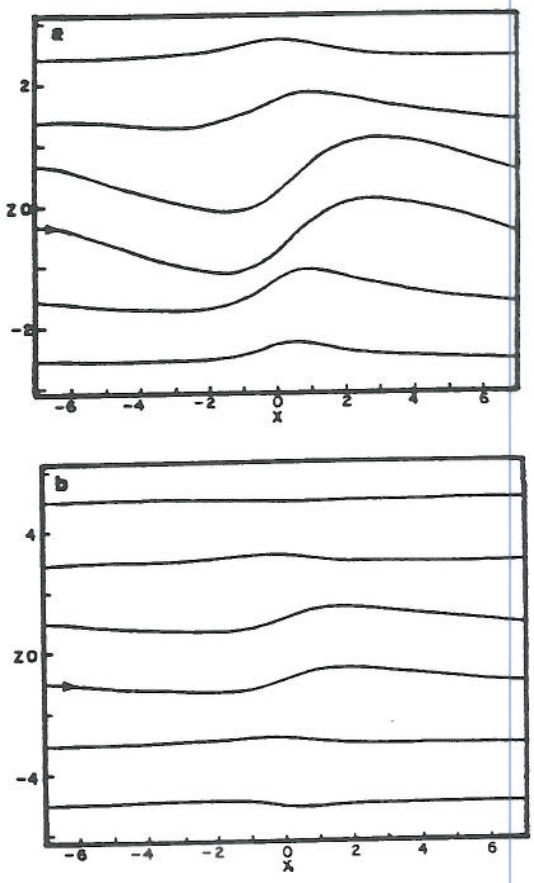

Fig. 37: (a) Vertical cross section along y=0 for Fig. 36 ($H=\pi$), (b) as in (a) except $H=2\pi$. (From Lin, 1986a)

$$c_{gx} = -\frac{\partial\omega}{\partial k} = \frac{-Nkm^2}{[k^2+l^2]^{1/2}\,[k^2+l^2+m^2]^{3/2}}, \tag{5.25a}$$

$$c_{gy} = -\frac{\partial\omega}{\partial l} = \frac{-Nlm^2}{[k^2+l^2]^{1/2}\,[k^2+l^2+m^2]^{3/2}}, \tag{5.25b}$$

$$c_{gz} = -\frac{\partial\omega}{\partial m} = \frac{N(k^2+l^2)^{1/2}\,m}{[k^2+l^2+m^2]^{3/2}}. \tag{5.25c}$$

For steady waves on a basic flow we replace ω with

the intrinsic frequency kU, so (5.24) becomes

$$m = \pm \frac{[(N^2-U^2k^2)(k^2+l^2)]^{1/2}}{kU} . \quad (5.26)$$

The components of the group velocity in a reference frame moving with the disturbance can be obtained by adding U to (5.25) and using (5.26):

$$c_{gx} = U\left(\frac{l^2 + k^4U^2/N^2}{k^2+l^2}\right) , \quad (5.27a)$$

$$c_{gy} = -U\left(\frac{lk(1 - k^2U^2/N^2)}{k^2+l^2}\right) , \quad (5.27b)$$

$$c_{gz} = \frac{U^2k^2(1 - k^2U^2/N^2)^{1/2}}{N^2(k^2+l^2)^{1/2}} . \quad (5.27c)$$

The wave energy propagates from the energy source along straight lines with slopes

$$\frac{x}{z} = \frac{c_{gx}}{c_{gz}} , \quad (5.28a)$$

$$\frac{y}{z} = \frac{c_{gy}}{c_{gz}} , \quad (5.28b)$$

$$\frac{y}{x} = \frac{c_{gy}}{c_{gx}} . \quad (5.28c)$$

With Eq. (5.28a,b), we obtain

$$\frac{y}{x} = -\frac{k(1 - k^2U^2/N^2)}{l(1 + k^4U^2/N^2l^2)} . \quad (5.29)$$

Use of Eqs. (5.29) and (5.28a) leads to

$$y^2 = \left(\frac{Nz}{U}\right)\left\{\frac{[1 - (kU/N)^2]^{3/2}}{(k^2+l^2)^{1/2}[1 + k^4U^2/N^2l^2]}\right\}x . \quad (5.30)$$

The above equation reduces to Eq. (31) of Smith (1980) in the hydrostatic limit, i.e., $k^2 << (N/U)^2$ for a uniform basic flow. For a certain height, the wave energy is concentrated near the parabola described by Eq. (5.30). However, the latus rectum becomes smaller compared to the hydrostatic case. The parabola becomes wider for higher altitudes, stronger stratification, and weaker basic wind.

To apply the above results to the real atmosphere, one has to consider a heat source distributed in a layer instead of being located at a certain level. For a heat source distributed uniformly from z_1 to z_2, the mathematical problem can be obtained by applying the Green's function method to the solution of Eq. (5.23)

$$\eta_1 = \iint_{-\infty}^{\infty} \frac{\hat{q}(K)\sin\lambda z\,(e^{i\lambda z_2} - e^{i\lambda z_1})}{k\left[1 - M^2(k-iv)^2\right]} e^{i(kx+ly)}dk\,dl \qquad 0 \le z < z_1$$

$$\eta_2 = \iint_{-\infty}^{\infty} \frac{-i\hat{q}(K)\,e^{i\lambda z}(\cos\lambda z - \cos\lambda z_1))}{k\left[1 - M^2(k-iv)^2\right]} e^{i(kx+ly)}dk\,dl + \iint_{-\infty}^{\infty} \frac{\hat{q}(K)\sin\lambda z\,(e^{i\lambda z_2} - e^{i\lambda z})}{k\left[1 - M^2(k-iv)^2\right]} e^{i(kx+ly)}dk\,dl \qquad z_1 \le z < z_2$$

$$\eta_3 = \iint_{-\infty}^{\infty} \frac{-i\hat{q}(K)\,e^{i\lambda z}(\cos\lambda z_2 - \cos\lambda z_1)}{k\left[1 - M^2(k-iv)^2\right]} e^{i(kx+ly)}dk\,dl \qquad z_2 \le z \quad (5.31)$$

The variables are nondimensionalized according to Eq. (5.22) except $\tilde{Q}_o = Q_o gb/(c_p T_o U^2 N)$. Figure 38 shows the vertical displacement for a hydrostatic flow over an elevated heat source distributed from z_1=1 to z_2=9. The dimensional flow parameters correspond to N=0.01 s^{-1}, z_1=1 km, z_2=9 km, b=5 km, and U=10 m s^{-1}. The nondimensional

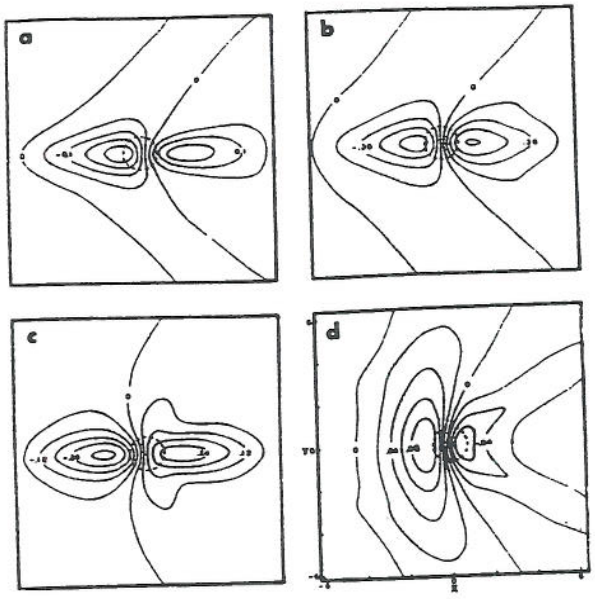

Fig. 38: Vertical displacement of a three-dimensional, continuously stratified, hydrostatic, uniform flow over an isolated heat source which is uniformly distributed from z_1=1 to z_2=9. The solution is given by Eq. (5.31) with M=0 and v=0.2. The four levels shown are: (a) 1, (b) 5, (c) 9, (d) 14. (From Lin, 1986a)

parameter M is set to 0 in this case. In the heating layer, the response of the airstream to the thermal forcing is a downward displacement upstream of the heating center followed by an upward displacement downstream. This is similar to the two-dimensional case discussed earlier. There exists no phase tilt in the heating layer. The vertical orientation of the disturbance is directly related to that of thermal forcing as demonstrated by Lin and Li (1988) (see their Fig. 3). As we move aloft to z=14 (Fig. 38d), V-shaped regions of upward and downward displacement are formed and located on the upwind and downwind sides of the heating center, respectively. The V-shaped regions are formed by the action of the basic wind on the direct and reflected upward propagating gravity waves. In relation to the thunderstorm generated V-shaped cloud tops, the cold (warm) area can be explained by the adiabatic cooling (warming) associated with the upward (downward) displacement. In addition, the upwind displacement of the cold area in the upper level with respect to the storm center may be explained as a gravity wave phenomenon.

The transient response of a hydrostatic airflow over a heat source has also been studied by Lin (1986a). A V-shaped region of upward displacement with an embedded region of downward displacement above the heating layer are produced. The whole system then advects downstream with a slower speed than the basic wind and eventually disperses.

Other mechanisms for the formation of V-shaped cloud tops have been proposed by others. Adler et al. (1981), Negri (1982), and Heymsfield et al. (1983a) proposed that the close-in warm area (Heymsfield and Blackmer, 1988) is produced by subsidence of negatively buoyant overshooting cloud air downshear of an ascending cloud top. Using a one-dimensional cloud model to simulate an overshooting cloud top, Adler and Mack (1986) suggested that mixing of the cloud air with the warmer stratospheric air is important in explaining the occurrence of the close-in warm point and the upwind offset of the cold point from the cloud summit. Schlesinger (1984, 1988) used a three-dimensional cloud model without ice processes to examine the origin of air in the cold and warm points associated with severe storm cloud tops. Schlesinger indicated that the strength of the cold-warm couplet is related to the magnitude of the shear in the near-tropopause region. The model showed that the warm area consisted of air parcels originating from both the updraft and stratospheric air above the cloud top

level. Schlesinger's results are consistent with the cloud dynamics arguments of Adler and Mack (1986). However, neither paper discussed the nature of the mixing processes and the ice processes are ignored in Schlesinger's model. The importance of the ice processes in thunderstorm dynamics has been demonstrated by Lin, Farley, and Orville (1983). Heymsfield et al. (1983b) offered another explanation in which the strong divergent outflows of the storms produce a variation in the ice content across the anvil top, such that higher concentrations of ice particles occurred in a V-shaped region. Heymsfield and Blackmer (1988) and Heymsfield et al. (1991) proposed a conceptual model in line with the wave theory of Lin (1986) and Lin and Li (1988). They suggested that the V-shaped cloud tops may be explained by the adiabatic cooling and warming associated with upward and downward motion of airflow over the cloud top which acts like a mountain. In reality, the cloud top may act like something in between a solid body and a "soft" warm air. In other words, the cloud should be represented by a thermal forcing which is also able to exert a drag on the environmental fluid such as a mountain.

The vertical velocity can be obtained immediately from the dimensional relationship $w'=U\partial\eta/\partial x$ for a steady flow. Figure 39 shows the vertical velocities at the heating base z_1 for (z_1, z_2) = (2,18), (1,9), (0.5,4.5), (0.25,2.25), and (0.125,1.125). The dimensional parameters may be considered as $N=0.01\ s^{-1}$, z_1=1 km, z_2=9 km, b=5 km, and U=5, 10, 20, 40, 80 m s^{-1}. For a fixed heating depth (dimensional), a smaller z_2-z_1 corresponds to a higher basic wind speed. Fig. 39b corresponds to the case of Fig. 38. The advection effect is more significant for cases with larger basic winds, which gives a more pronounced V-shaped pattern. This

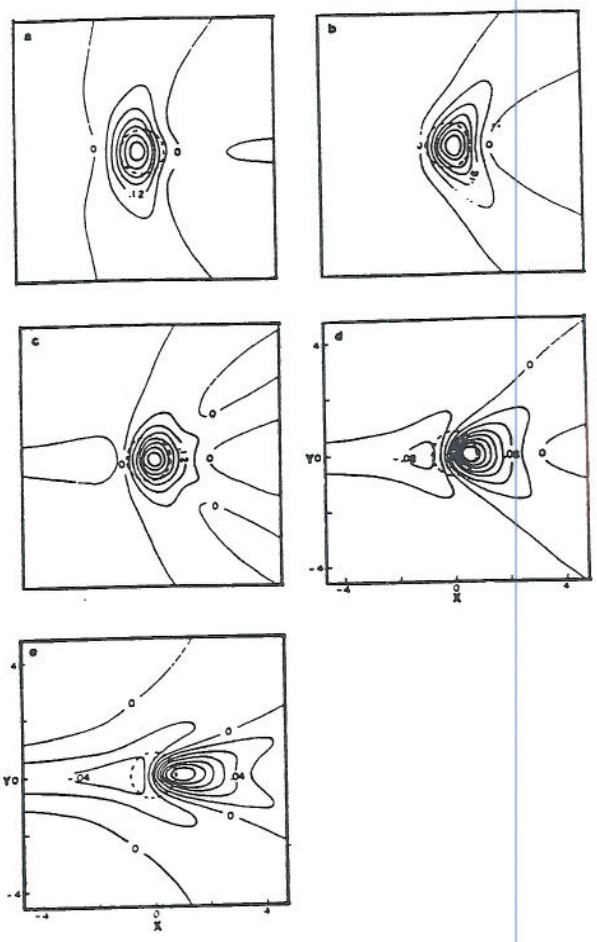

Fig. 39: Vertical velocity at $z=z_1$ of a three-dimensional, continuously stratified, hydrostatic, uniform flow over a heat source which is uniformly distributed from z_1 to z_2. The solution is given by Eq. (5.31) with M=0 and ν=0.2. The four cases of different (z_1,z_2) shown are: (a) (2,18), (b) (1,9), (c) (0.5, 4.5), (d) (0.25, 2.25), and (e) (0.125, 1.125). (From Lin, 1986a)

figure indicates that an upward motion at the cloud base as required by a wave-CISK mechanism may be satisfied with a wide variety of the basic wind speeds

in the present model. Although, the air still has to overcome the downward displacement established upstream of the heating region, as pointed out by Raymond (1986).

In a study of three-dimensional inviscid airflow over an isolated mountain, Smolarkiewicz and Rotunno (1989) found that a pair of vortices form on the lee side of the mountain in a low Froude number (Fr=U/Nh < 0.5) flow. The formation of these lee vortices are explained by the tilting of horizontal vorticity produced baroclinically in an inviscid continuously stratified fluid. Smith (1989) commented that the lee vortices can be generated by either a density surface interaction or by overturning and turbulence in an inviscid fluid. It is suspected here that a similar phenomenon may occur in an inviscid flow over a heating source or sink. However, this hypothesis remains to be tested. A nonlinear model is needed to examine the possibility of the formation of vortices on the lee of heat source or sink. With the Coriolis force included in a study similar to Smolarkiewicz and Rotunno, Lin et al. (1992) demonstrated that a lee mesocyclone can be generated in a three-dimensional, inviscid, low Froude number flow past an isolated mountain. A similar analogy may be drawn for a flow over a meso-β/α scale heat source or sink. If a mesocyclone forms, it may be related to the formation of coastal cyclones. Again, it remains to be investigated in further studies.

b. Shear Flow with a Critical Level

The theory developed in the last section may be extended to include a multi-directional shear flow with a critical level. The governing equation is a combination of Eqs. (5.1) and (5.15)

$$\left(U\frac{\partial}{\partial x}+V\frac{\partial}{\partial y}+\nu\right)^2\nabla^2 w' - \left(U\frac{\partial}{\partial x}+V\frac{\partial}{\partial y}+\nu\right)\left(U_{zz}\frac{\partial}{\partial x}+V_{zz}\frac{\partial}{\partial y}\right)w' + N^2\nabla_H^2 w' = \frac{g}{c_pT_o}\nabla_H^2 q' \tag{5.32}$$

After making the double Fourier transform in x (--> k) and y (--> l), the above equation becomes

$$\hat{w}_{zz} + \left\{\frac{-(kU_{zz}+lV_{zz})}{kU+lV-i\nu} + \left(\frac{N^2}{(kU+lV-i\nu)^2} - 1\right)K^2\right\}\hat{w} = \frac{gK^2}{c_pT_o(kU+lV-i\nu)^2}\hat{q}(k,l,z) \tag{5.33}$$

Again the heating can be assumed to be a bell-shaped function in x and y and uniformly distributed in vertical. The mathematical problem is complicated. Thus, a simple numerical technique may be adopted to obtain the solution which can provide a physical solution to the problem. Eq. (5.33) in the Fourier space is a special case of the general form of the Taylor-Goldstein equation

$$\zeta_{zz} + p(z)\,\zeta = r(z) \tag{5.34}$$

with the boundary conditions

$$\zeta(z_o) = \zeta_o \quad \text{at } z=z_o$$
$$\zeta(z_T) = \zeta_T \quad \text{at } z=z_T, \tag{5.35}$$

where the subscripts o and T represent the lower and upper boundaries, respectively. Applying a center-difference numerical scheme to the above equation yields

$$\begin{aligned}
&(-2\zeta_1 + \zeta_2) + h^2 p_1\zeta_1 = h^2 r_1 - \zeta_o \\
&(\zeta_{i-1} - 2\zeta_i + \zeta_{i+1}) + h^2 p_i\zeta_i = h^2 r_1, \quad i=2,3,\ldots,n-1 \\
&(\zeta_{n-1} - 2\zeta_n) + h^2 p_n\zeta_n = h^2 r_n - \zeta_T
\end{aligned} \tag{5.36}$$

where h is the interval for numerical integration. In the following examples, the h and horizontal grid interval are chosen to be 250 and 1500 m, respectively. The above linear system can be solved

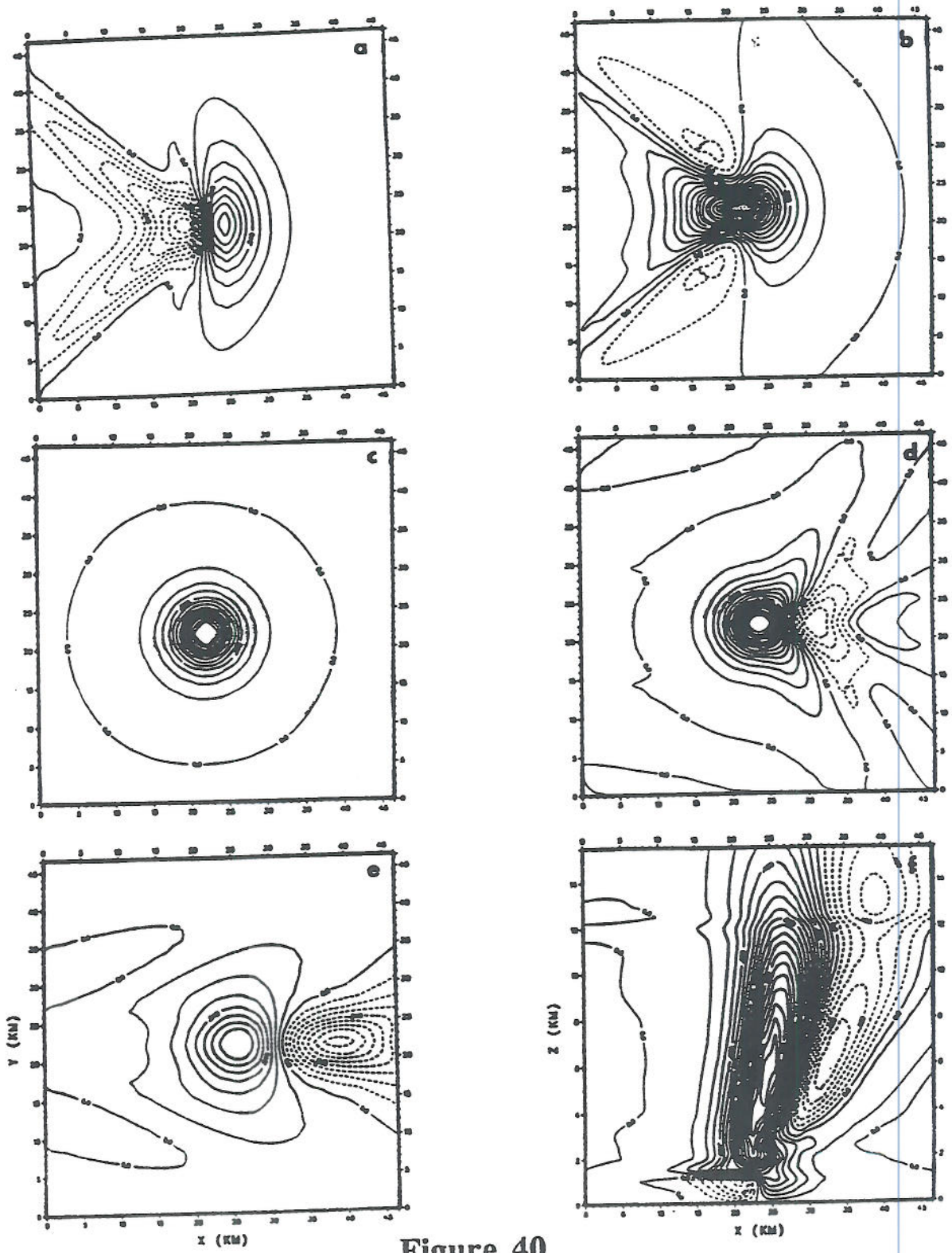

Figure 40

by applying the Gaussian elimination scheme to the banded matrix column vector $[\zeta_1, ..., \zeta_n]$ as long as the boundary conditions are known. The upper radiation boundary condition is simulated by a sponge layer (Klemp and Lilly, 1978) in which the coefficient of Rayleigh friction and Newtonian cooling is gradually increased by a factor of 5 in the sponge layer according to a sine square function. Once the numerical solution in the Fourier space is obtained, then a two-dimensional FFT algorithm can be adopted to invert the solution back to the physical space.

Figure 40 shows the flow fields for a nonhydrostatic shear flow over an elevated heat source. A linear shear, $U(z)=-U_o+(U_o/z_c)z$ and $V(z)=0$, is assumed in this case. The critical level (z_c) is located at 2 km. Other parameters chosen are: $N=0.01\ s^{-1}$, $U_o=10\ m\ s^{-1}$, $Q_o=4\ J\ kg\ s^{-1}$, $b=5$ km, $z_1=1.5$ km, $z_2=12$ km, and $\nu=10^{-4}\ s^{-1}$. A rather small heating rate is used to avoid the violation of the small amplitude assumption. The cloud base and top can be assumed to be 1 km and 14 km, respectively. Even though these values are not involved in the calculation, it should be noted that the cloud base and top are not necessarily located exactly at the same height as the heating base and top, respectively. The Richardson number associated with the basic flow is 4. The grid resolution is 64 x 64 x 101. The actual horizontal domain is 94.5 km x 94.5 km. Ony the central portion, 46.5 km x 46.5 km, are shown in the figure. The horizontal domain is chosen to be large enough so that the effect of periodic conditions assumed by the FFT algorithm can be minimized. The vertical extent of the physical layer is 15 km, while the sponge layer extends from 15 km to 25 km.

At the cloud base (z=1km), the basic wind blows from right to left. Upward motion is generated upstream of the heating center with downward motion downstream of the heating. The region of upward motion forms a V-shaped pattern with the vertex pointing upstream. The V-shaped pattern of upward velocity in the low levels have also been found in numerical simulations (e.g., Klemp and Wilhelmson, 1978; Schlesinger, 1980). The formation of this V-shaped pattern is similar to that discussed in the last section except with downward propagating gravity waves. Evidence of these downward propagating waves is also shown in the upstream shift of the maximum updraft from Fig. 40a, b and f. At the heating base z_1 (Fig. 40b), the heating region is dominated by upward motion. The colocation of the upward motion and the heating at the heating base is important in supporting the existing convection. Moving further aloft to the critical level, z_c=2km, the response of the airflow to

Fig. 40: Vertical velocity fields for a nonhydrostatic continuously stratified shear flow over an elevated heat source. The critical level (z_c) is located at 2 km. The solution is given by Eq. (5.33) solved by the numerical scheme Eq. (5.36) and an FFT algorithm. Other parameters chosen are: $N=0.01\ s^{-1}$, $U_o=10\ m\ s^{-1}$, $Q_o=4\ J\ kg\ s^{-1}$, $b=5$ km, $z_1=1.5$ km, $z_2=12$ km, and $\nu=10^{-4}\ s^{-1}$. The Richardson number associated with the basic flow is 4. Five levels are shown for : (a) 1 km, (b) 1.5 km (z_1), (c) 2 km (z_c), (d) 5 km, and (e) 14 km. The vertical cross section along y=0 is shown in (f). Units for the vertical velocity is in $m\ s^{-1}$. (From Lin and Li, 1988)

the diabatic heating is an axisymmetric region of upward motion (Fig. 40c). Similar to the two-dimensional case (Eq. (5.14)), the vertical velocity at the critical level is directly proportional to the heating according to the thermodynamic equation since the basic wind vanishes there. Thus, the region of upward motion reproduces the bell-shaped pattern of the heat source. Notice that the basic wind profile used in this case agrees better with squall lines and multicell storms than right or left moving supercells, which would maintain a constant storm-relative V-component $V(z)=\pm V_0$ to the wind. The gravity wave pattern produced by this type of supercells is better represented in Lin (1986a) and Raymond (1986). The positive response of vertical motion at the cloud base depends upon the heating-induced Froude number $[F=U/N(z_2-z_1)]$, which corresponds to the wave-CISK modes (Raymond, 1986). At higher levels, such as 5 and 14 km (Fig. 40d and e), the V-shaped regions of upward motion are pronounced. This result is consistent with the non-sheared case studied in Lin (1986a) and with numerical modeling studies of Klemp and Wilhelmson (1978) and Schlesinger (1988). The vertical motion is weaker at 14 m than at lower levels because of the divergence above the heating region and the viscosity. Due to the nonhydrostatic effect, repeating, damped oscillations of the disturbance may be produced (e.g., Fig. 2e of Lin and Li, 1988). The formation of V-shaped patterns of vertical velocity is explained earlier by Eq. (5.30).

The vertical cross section of vertical velocity along y=0 is shown in Fig. 40t. In the concentrated heating region, the vertical velocity is positive in the heating layer, with a maximum located at about 5.5 km. The vertical orientation of the updraft core depends on the vertical shear of the environmental wind. The slightly downshear tilt is due to the strong advection of the basic wind. For a relatively weak shear case, the updraft is almost erect. The upstream tilt of the vertical velocity above the heating top (12 km) is offset by the advection effect (Fig. 40f). The downward motion on the downshear side (right side in Fig. 40f) of the updraft is evidence for the existence of the thermally forced gravity wave. Below the cloud base (1 km), the updraft is shifted upstream followed by a downdraft region. This sloping updraft near the cloud base may enhance the formation of new convective cells. These new convective cells may develop to be part of the supercell or as a short-lived cell in a long-lived convective system (Rotunno et al., 1988).

The propagation of wave energy induced by a stationary heat source in an unbounded, steady stratified shear flow is sketched in Fig. 41. At upper levels, the energy propagates upward and upstream relative to the air (c_{ga}), but is advected downstream by the basic wind. Thus, the wave energy is found to be along the direction of c_{gh+} or c_{gh-} relative to the heat source. The formation of the repeating, damped oscillations of the disturbance (Fig. 40f) is mainly caused by the nonhydrostatic effect. Similar to mountain wave theory (Smith, 1979), this nonhydrostatic wave only occurs when the dominant squared wave number (K^2) is less than the Scorer parameter ($N^2/U^2(z)$) for a Boussinesq, constant shear flow. This result also can be explained by the group velocity argument. For simplicity, let us consider a corresponding two-dimensional flow for which Eq. (5.28a) reduces to

$$\frac{z}{x}=\left(\frac{N}{U}\right)\frac{\left(1-k^2U^2/N^2\right)^{1/2}}{k} \tag{5.37}$$

The wave energy propagates along the straight line given by the above equation, emanating from the origin where the heat source is located. Now it

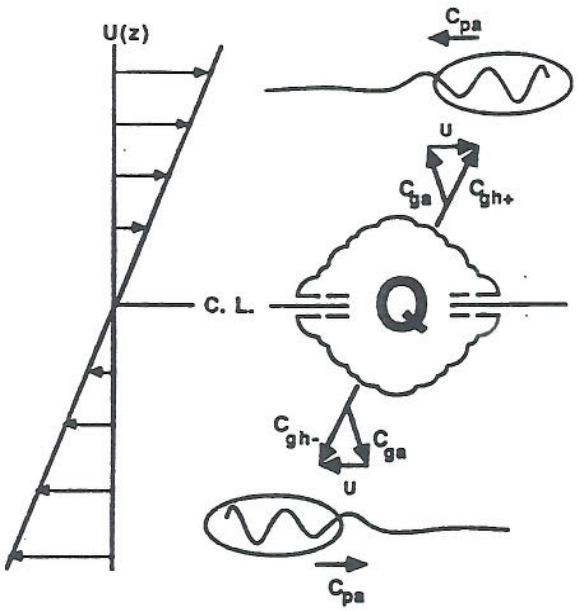

Fig. 41: A sketch for the propagation of wave energy associated with steady waves forced by a prescribed heating in an unbounded, nonhydrostatic continuously stratified shear flow. Symbols c_{pa}, c_{ga}, c_{gh+}, and c_{gh-} represent the phase velocity with respect to (w.r.t.) the air, group velocity w.r.t. the air, upward group velocity w.r.t. the heat source, and downward group velocity w.r.t. the heat source. (From Lin and Li, 1988)

becomes clear that in order to have the wave energy propagate downstream (x>0) and upward (z>0), it requires that $K^2<N^2/U^2(z)$. To determine the control parameter of the downstream wavelength of the heating-induced gravity wave, we assume that the wavelength at a certain height z* above the critical level (denoted by C.L. in Fig. 41) is L. Thus, x*, k*, and U(z) are equal to L, $2\pi/L$ and $U_z z$, respectively. Substituting z*, x*, and k* into Eq. (5.37) and solving for L, we obtain

$$L = \frac{\sqrt{2}\pi z}{Ri^{1/2}} \left[1 \pm \sqrt{(1 + Ri/\pi^2)} \right]^{1/2}$$

Thus, the downstream wavelength is approximately proportional to $Ri^{-1/2}$ for a stable flow with a relatively strong shear ($Ri << \pi^2$). A rough estimate from Fig. 40f gives L=34 km for Ri=4. This result is consistent with the above conclusion.

Figure 42 shows a case with a multi-directional shear. The hodograph is depicted in Fig. 42e. At the cloud base, 1 km, the basic wind blows from the southeast (Fig. 42a). The regions of upward and downward motion are located on the upwind and downwind sides, respectively. The extrema of the vertical velocity are lined up along the direction of the basic environmental wind. The vertical velocity field shows an asymmetric pattern which is caused by weak advection of gravity waves by the north-south component of the basic wind. This asymmetry is also shown in the field of vertical displacement (Fig. 42b). In the vicinity of the heating region, the flow is dominated by an upward displacement. The downward displacements on the upstream (southeast) and downstream (northwest) sides are relatively small compared with the upward displacement. Even though the north-south wind is relatively weak at the cloud top level (14 km), asymmetric patterns are still pronounced in the fields of vertical velocity and displacement (Fig. 42c and d). Thus, the thermally forced gravity waves in a multi-directional shear help to explain (Heymsfield et al., 1983a; Lin and Li, 1988) the asymmetric pattern of V-shaped cloud tops, such as those observed by Anderson (1982).

6. Three-Dimensional Flow over a Meso-α/β Heat Source

For a stably stratified flow over a diabatic heat source or sink with a horizontal scale on the order of

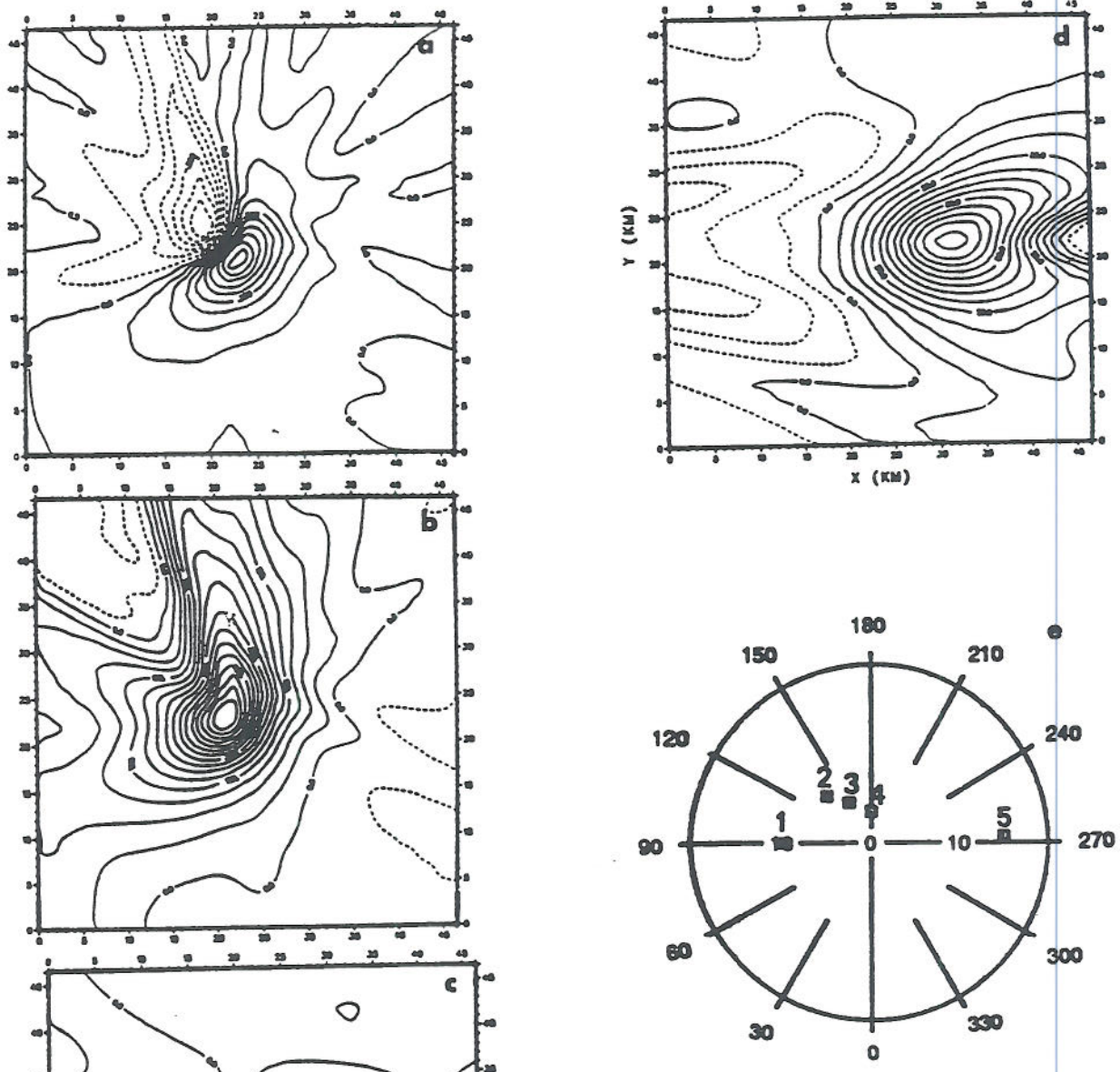

Fig. 42: As in Fig. 40 except with a multidirectional shear as sketched in the hodograph (e). Fields plotted are: (a) w' at 1 km (cloud base), (b) η at 1 km, (c) w' at 14 km (cloud top), and (d) η at 14 km. (From Lin and Li, 1988)

one hundred kilometers, the rotational effect plays an important role in generating inertia-gravity waves. Those waves behave differently from pure gravity waves which are generated by a heat source or sink with a horizontal scale on the order of ten kilometers or smaller. They are also different from quasi-geostrophic planetary waves which are generated by a heat source or sink with a horizontal scale on the order of thousand kilometers. In this type of flow, the β-effect may be neglected, but the inertial effects should be included.

By prescribing an isolated diabatic heat source/sink, Rotunno (1983) has investigated the rotational effects on the land and sea breeze circulation theoretically. Using a similar approach, Hsu (1987a) has studied the two-dimensional flow response to a prescribed, finite surface heating with Fickian thermal diffusion included. The horizontal scale of the heating varies from 1 to 1000 km. This work was extended numerically to include the three-dimensionality and applied to the snowstorm problem of Lake Michigan (Hsu, 1987b). Some interesting results have been found by Hsu by varying the shape of the diabatic heating and the basic wind directions. However, the energy propagation of the heating-induced inertia-gravity waves has not been emphasized, which need to be investigated for a better understanding of the dynamics. Using a linear theoretical model, Luthi et al. (1989) studied the nature and the flow response to prescribed low-level, mesoscale steady state diabatic heating with Rossby numbers greater and smaller than 1. They found that the response is strongly sensitive to: the horizontal scale of the diabatic region, three-dimensional effects, basic rotation of the flow system and the strength of the momentum and thermal damping. The inertial effects of a three-dimensional uniform flow over a mesoscale heat source have been investigated by Lin (1989a) by comparing the response with that of a quasi-geostrophic flow. This work will be reviewed in this section.

The above problem is related to the shear flow over the East Coast of the United States. Cyclogenesis along the east coast of the United States has received considerable attention since the recent completion of the Genesis of Atlantic Lows Experiment (GALE). These cyclones often form off the Carolina coast, develop rapidly, and move northeastward, which may bring heavy snowfall and damage over the mid-Atlantic states. Different kinds of approaches, such as observational data analysis (e.g., Bosart, 1981; Uccellini et al., 1984), numerical simulations (e.g., Anthes et al., 1983; Orlanski and Katzfey, 1987) and theoretical studies (e.g., Smith, 1986; Lin, 1989b, 1990a), have been used to investigate the problem of East Coast cyclogenesis. Observational studies suggest that there are two major mechanisms responsible for the East Coast cyclogenesis. The first may be called the boundary-layer control of cyclogenesis (e.g., Bosart, 1981; 1988). It is proposed that the cyclonically curved coastline under a northeasterly flow is favorable for the growth of cyclonic vorticity in response to differential heating and differential friction between a relatively warm ocean and colder landmasses. The second mechanism may be called the upper-level jet streak/trough control of cyclogenesis (e.g., Uccellini et al., 1984; Uccellini and Kocin, 1987). It is proposed that the circulation patterns associated with jet streaks establish an environment within which low-level processes can further contribute to cyclogenesis. The transverse ageostrophic components associated with jet streaks aloft combine with the longitudinal components associated with trough-ridge systems and can

provide for the upper-level divergence conducive to surface cyclogenesis as envisioned by Bjerknes (1951). It appears that the boundary-layer mechanism is more responsible for the early formation of the coastal cyclone, while the upper-level forcing mechanism is more responsible for the later development. One example is the case of GALE IOP#2 (GALE, 1986), in which there are no migratory shortwave trough/jet streaks aloft to account for the cyclogenesis at the early stage. As a shortwave trough aloft moves over the genesis region at a later time, the cyclone then begins to move northeastward and develops further along the coastal front. In order to understand the effect of differential heating on the development of a coastal cyclone, it is important to study the response of a baroclinic flow to a low-level heating. In this paper, we will review the responses of a baroclinic flow over a prescribed low-level heat source studied by Lin (1989b; 1990a) and some recent results.

6.1 Steady Barotropic Flow

The small-amplitude equation of vertical velocity for a steady, three-dimensional, stratified, hydrostatic Boussinesq flow in a rotating system may be written

$$Uu'_x - fv' = -(1/\rho_o)\, p'_x \tag{6.1}$$

$$Uv'_x + fu' = -(1/\rho_o)\, p'_y \tag{6.2}$$

$$p'_z = (g\rho_o/\theta_o)\,\theta' \tag{6.3}$$

$$u'_x + v'_y + w'_z = 0 \tag{6.4}$$

$$U\theta'_x + (\theta_o N^2/g)\, w' = (\theta_o/c_p T_o)\, q' . \tag{6.5}$$

The above equations may be nondimensionalized by

$(\tilde{x}, \tilde{y})=(x/b, y/b)$; $\tilde{z}=z/H_o$; $(\tilde{u},\tilde{v})=(u'/U, v'/U)$; $\tilde{w}=w'b/(R_o U H_o)$; $\tilde{p}=p'/(\rho_o f U b)$; $\theta=(\theta' g H_o)/(f\theta_o U b)$;

$$\tilde{q} = q' g H_o/(c_p T_o U^2 f), \tag{6.6}$$

to yield (with tildes dropped)

$$R_o u_x - v + p_x = 0 \tag{6.7}$$

$$R_o v_x + u + p_y = 0 \tag{6.8}$$

$$p_z - \theta = 0 \tag{6.9}$$

$$u_x + v_y + R_o w_z = 0 \tag{6.10}$$

$$\theta_x + w = q, \tag{6.11}$$

where b is the horizontal scale of the heat source, $R_o=U/fb$ and $H_o=fb/N$ are the Rossby number and the deformation depth (e.g. see Buzzi and Tibaldi, 1977; Pierrehumbert and Wyman, 1985).

To investigate the inertial effects, we consider the flow response in a quasi-geostrophic system. This will provide a basis for comparison. Eqs. (6.7)-(6.11) can be reduced to a single equation for the pressure perturbation by making the quasi-geostrophic approximation, i.e. retaining the zeroth and first order terms in a Taylor series expansion of the dynamical variables in powers of R_o (for details, see Pedlosky, 1982)

$$\frac{\partial}{\partial x}(p_{zz} + \nabla_H^2 p) = q_z . \tag{6.12}$$

The lower boundary, with Ekman friction (Charney and Eliassen, 1949) included, requires

$$w' = -\left(\frac{U}{\rho_o N^2}\right) p'_{xz} + \left(\frac{g}{c_p T_o N^2}\right) q' = H_o\left(\frac{1}{2}E^{1/2}\right)\zeta' \quad \text{at } z=0, \tag{6.13}$$

where $E=\nu/(fH_o^2)$ is the Ekman number and ζ' is the vertical component of the relative vorticity. The nondimensional form of the above equation is

$$p_{xz} + [(E^{1/2}/2)/R_o]\,\zeta = q \quad \text{at } z=0. \tag{6.14}$$

For a low-level thermal forcing, we may assume

$$q'(x, y, z) = h'(x, y)\, e^{-z/H_1}, \tag{6.15}$$

where h'(x, y) is the horizontal distribution of the heating and H_1 is the e-folding depth of the heating. The above equation can be expressed in nondimensional form

$$q(x, y, z) = h(x,y)\, e^{-z/\gamma}, \tag{6.16}$$

where $\gamma = H_1/H_o = NH_1/fb$ is the aspect ratio of the heating depth to the deformation depth.

To solve the problem, we make the double Fourier transform in x and y of Eqs. (6.12), (6.14), and (6.16)

$$\hat{p}_{zz} - K^2\hat{p} = -\left(\frac{\hat{h}}{i\gamma k}\right) e^{-z/\gamma}, \tag{6.17}$$

with

$$\hat{p}_z - \left\{\frac{(1/2)E^{1/2}K^2}{R_o ik}\right\}\hat{p} = \frac{\hat{h}(k,l)e^{-z/\gamma}}{ik} \quad \text{at } z=0. \tag{6.18}$$

The general solution of Eq. (6.17) can be written

$$\hat{p} = Ae^{-Kz} + Be^{Kz} - \frac{\hat{h}\gamma e^{-z/\gamma}}{ik\,(1 - \gamma^2 K^2)}. \tag{6.19}$$

The upper boundary condition requires p --> 0, which implies B=0. After applying the lower boundary condition (6.18), the solution in the Fourier space can be obtained

$$\hat{p} = \frac{\hat{h}\gamma}{ik(1-\gamma^2K^2)}\left\{K\left[\gamma + \frac{(E^{1/2}/2)(1-\gamma K)}{R_o ik + (E^{1/2}/2)K}\right]e^{-Kz} - e^{-z/\gamma}\right\}. \tag{6.20}$$

Other variables are related to p by the following relationships:

$$w = -p_{xz} + q, \quad u = -p_y, \quad v = p_x,$$
$$\zeta = \nabla_H^2 p, \quad \delta = R_o\,(p_{xzz} - q_z), \tag{6.21}$$

where ζ and δ are the vertical component of relative vorticity and the horizontal divergence, respectively. The vertical velocity in the Fourier space can then be obtained by using Eqs. (6.20) and (6.21).

Again, we assume a bell-shaped warm region associated with low-level sensible heating,

$$T'(x, y) = \frac{T'_o}{(r^2/b^2+1)^{3/2}}, \tag{6.22}$$

To a first approximation, the diabatic heating rate associated with the above specified warm region in a basic flow (U) can be specified as

$$\frac{q'}{c_p} = \frac{D\theta}{Dt} = U\frac{\partial T'}{\partial x} + \left(\frac{N^2\theta_o}{g}\right) w'. \tag{6.23}$$

As discussed in Stern and Malkus (1953), the diabatic heating rate is mainly created and maintained by horizontal temperature advection due to small-scale turbulence, and is not altered significantly by convective motions of the scale of w'. Thus, the last term of the above equation may be neglected. After making the Fourier transform of Eq. (6.22) and the approximated form of Eq. (6.23), we have

$$\hat{h}(k, l) = iT_o k e^{-K}/2\pi. \tag{6.24}$$

Substituting Eq.(6.24) into Eqs. (6.20) and (6.21) in Fourier space, the variables $\hat{p}$, $\hat{w}$, $\hat{u}$, $\hat{v}$, $\hat{\zeta}$, and $\hat{\delta}$ can be solved analytically in the Fourier space and then transformed back to the physical space numerically using a Fast Fourier transform (FFT) algorithm.

Figure 43 shows a case of quasi-geostrophic inviscid flow over an isolated warm region which has a maximum temperature and a half-width of 7.5 and 1, respectively. The basic flow blows from the left to right. According to Eq. (6.23), there exists heating (cooling) upstream (downstream) of the

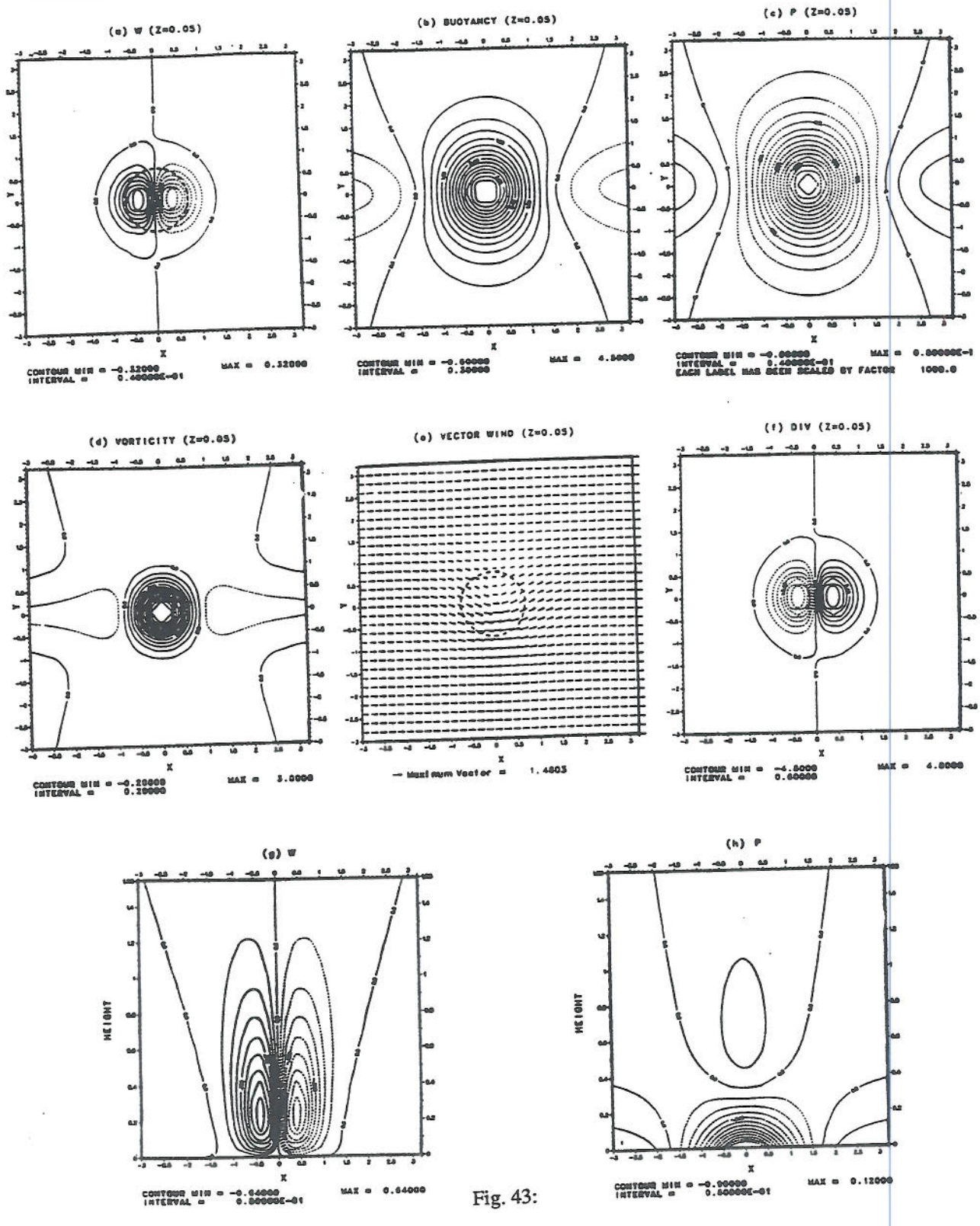
(a) W (Z=0.05)
(b) BUOYANCY (Z=0.05)
(c) P (Z=0.05)
(d) VORTICITY (Z=0.05)
(e) VECTOR WIND (Z=0.05)
(f) DIV (Z=0.05)
(g) W
(h) P
HEIGHT
X
Y

Fig. 43:

center of the warm region. Both R_o and γ have a value of 0.2. The dimensional parameters may be considered as U=10 ms^{-1}, b=500 km, f=10^{-4} s^{-1}, N=0.01 s^{-1}, H_1=1 km, H_o=5 km, and T'_o=20 K. The response of the atmosphere to the heating and cooling associated with the warm region at z=0.05 (250 m) is an upward (downward) motion upstream (downstream) of the center of the warm region (Fig. 43a). Upstream (downstream) of the region of upward (downward) motion, there exists a region of weak compensating downward (upward) motion. In fact, the vertical velocity field is in phase with the diabatic heating. The thermal forcing produces a region of high buoyancy (less dense) air in the vicinity of the warm region (Fig. 43b). The buoynacy is defined as $g\theta'/\theta_o$, which then produces the low pressure region near the surface (Fig. 43c) as required by the hydrostatic balance. On both upstream and downstream sides of the region of high buoyancy and low pressure, there exist regions of weak low buoyancy and high pressure, respectively. At this level (z=0.05), the air parcel experiences a cyclonic circulation near the center of the low pressure region where there exists a cell of positive relative vorticity (Fig. 43d and e). Two regions of weak negative vorticity appear to be on both upstream and downstream sides of the positive vorticity. Notice that the relative vorticity reaches a maximum of about 0.6f, which is relatively high for the quasi-geostrophic approximation to be valid. Fig. 43f shows the divergence field at z=0.05, which has a convergence (divergence) upstream (downstream) of the center of the warm region. The divergence field is related to the vertical motion by the relationship $\delta=-w_z$.

Fig. 43g and h displays the vertical cross sections of the vertical velocity and perturbation pressure along y=0. The vertical velocity field (Fig. 43g) near the warm region center is mainly dominated by an upward motion upstream followed by a downward motion. The absolute value of the vertical velocity increases with height until z=0.2 and then decreases. Weak compensative downward and upward motions are found far upstream and downstream, respectively. The air parcel is lifted near the center of the warm region and displaced slightly downward far upstream and downstream. There exists strong vortex stretching near the center of the warm region and two regions of weak vortex compression far upstream and downstream. The pressure perturbation (Fig. 43h) is almost confined below the e-folding depth of the heating, i.e. z=0.2. Near the warm region center, the perturbation pressure decreases exponentially with height and reverses its phase at a level of about z=0.35. The resulting high pressure is associated with the compensative divergence at this level, instead of convergence at the lower level. The amplitude of the perturbation pressure decays exponentially with height as also can be detected from the solution,

Fig. 43: Inviscid quasi-geostrophic barotropic flow over a bell-shaped warm region with the maximum perturbation potential temperature (T_o) and the half-width (b) of 7.5 and 1, respectively. The parameters associated with the basic flow are: R_o=0.2, γ=0.2, E=0. Six horizontal fields at z=0.05 are shown: (a) vertical velocity, (b) buoyancy , (c) perturbation pressure, (d) relative vorticity, (e) horizontal vector wind, and (f) divergence. Three cross sections along y=0 are shown: (g) vertical velocity and (h) perturbation pressure. The thick dashed lines in (a) and (e) indicate the contour of T=4. Notice that all variables are nondimensionalized. (From Lin, 1989a)

Eq.(6.20).

To investigate the inertial effects, we may combine Eqs. (6.6)-(6.10) into a single equation for w,

$$R_o^2 w_{xxzz} + w_{zz} + \nabla_H^2 w = \nabla_H^2 q. \tag{6.25}$$

Making Fourier transforms of the above equation and Eq. (6.16) gives

$$\hat{w}_{zz} + \frac{K^2}{R_o^2 k^2 - 1}\hat{w} = \frac{\hat{h} K^2 e^{-z/\gamma}}{R_o^2 k^2 - 1}. \tag{6.26}$$

The general solution of the above equation can be written

$$\hat{w} = A \exp(iKz/\sqrt{(R_o^2 k^2 - 1)}) + B \exp(-iKz/\sqrt{(R_o^2 k^2 - 1)}) + \frac{\hat{h}\gamma^2 K^2 e^{-z/\gamma}}{\gamma^2 K^2 + (R_o^2 k^2 - 1)} \tag{6.27}$$

The lower boundary condition requires w=0 at z=0. The solution composes two parts: (a) $R_o^2 k^2 > 1$ and (b) $R_o^2 k^2 < 1$. For $R_o^2 k^2 > 1$, the upper boundary condition requires B=0 for allowing the energy to radiate upward to infinity. Thus, the solution in this upward propagating wave regime can be obtained

$$\hat{w} = \frac{-\hat{h}\gamma^2 K^2}{\gamma^2 K^2 + (R_o^2 k^2 - 1)} [e^{iKz/(R_o^2 k^2 - 1)^{1/2}} - e^{-z/\gamma}], \quad \text{for } R_o^2 k^2 > 1 \tag{6.28}$$

The solution in the other regime ($R_o^2 k^2 < 1$) can be obtained in a similar way except it requires the solution to vanish at infinity. As discussed in Section 2, this regime is called the evanescent wave regime. The solution reads

$$\hat{w} = \frac{-\hat{h}\gamma^2 K^2}{\gamma^2 K^2 - (1 - R_o^2 k^2)} [e^{-Kz/(1 - R_o^2 k^2)^{1/2}} - e^{-z/\gamma}], \quad \text{for } R_o^2 k^2 < 1 \tag{6.29}$$

The other variables can be obtained

$$\hat{p} = \frac{1}{ik}\left[\int_z^{\infty} \hat{w}\, dz - \int_z^{\infty} \hat{h} e^{-z/\gamma} dz\right], \tag{6.30}$$

$$\hat{u} = \frac{R_o^2 k^2 - il}{1 - R_o^2 k^2}\hat{p}, \tag{6.31}$$

$$\hat{v} = \frac{R_o^2 kl + ik}{1 - R_o^2 k^2}\hat{p}, \tag{6.32}$$

$$\hat{b} = \frac{1}{ik}(\hat{q} - \hat{w}), \tag{6.33}$$

$$\hat{\zeta} = -K^2\hat{p} - iR_o^2 k\hat{w}_z, \tag{6.34}$$

$$\hat{\delta} = -R_o\hat{w}_z. \tag{6.35}$$

Figure 44 shows an example of an inviscid flow with R_o=1 past an isolated warm region. The parameters associated with the flow and the diabatic source/sink are γ=1 and T_o=1.5. The dimensional parameters may be considered as U=10 ms^{-1}, b=100 km, f=10^{-4} s^{-1}, N=0.01 s^{-1}, H_1=1 km, H_o=1 km, and T_o=4 K. The response of the fluid to the diabatic heating at z=0.25, corresponding to a dimensional height of 250 m, is an upward motion upstream and near the center of the warm region followed by a downward motion downstream (Fig. 44a). Compared with the quasi-geostrophic case (Fig. 43), the major regions of upward and downward motion are shifted downstream. This can be explained by the advection effect because the inertial terms, i.e. the R_o terms, play a significant role in the present case. Even though not shown in Fig. 44a, there still exists a weak compensative downward motion associated with the major region of upward motion (Fig. 44g). The horizontal pattern

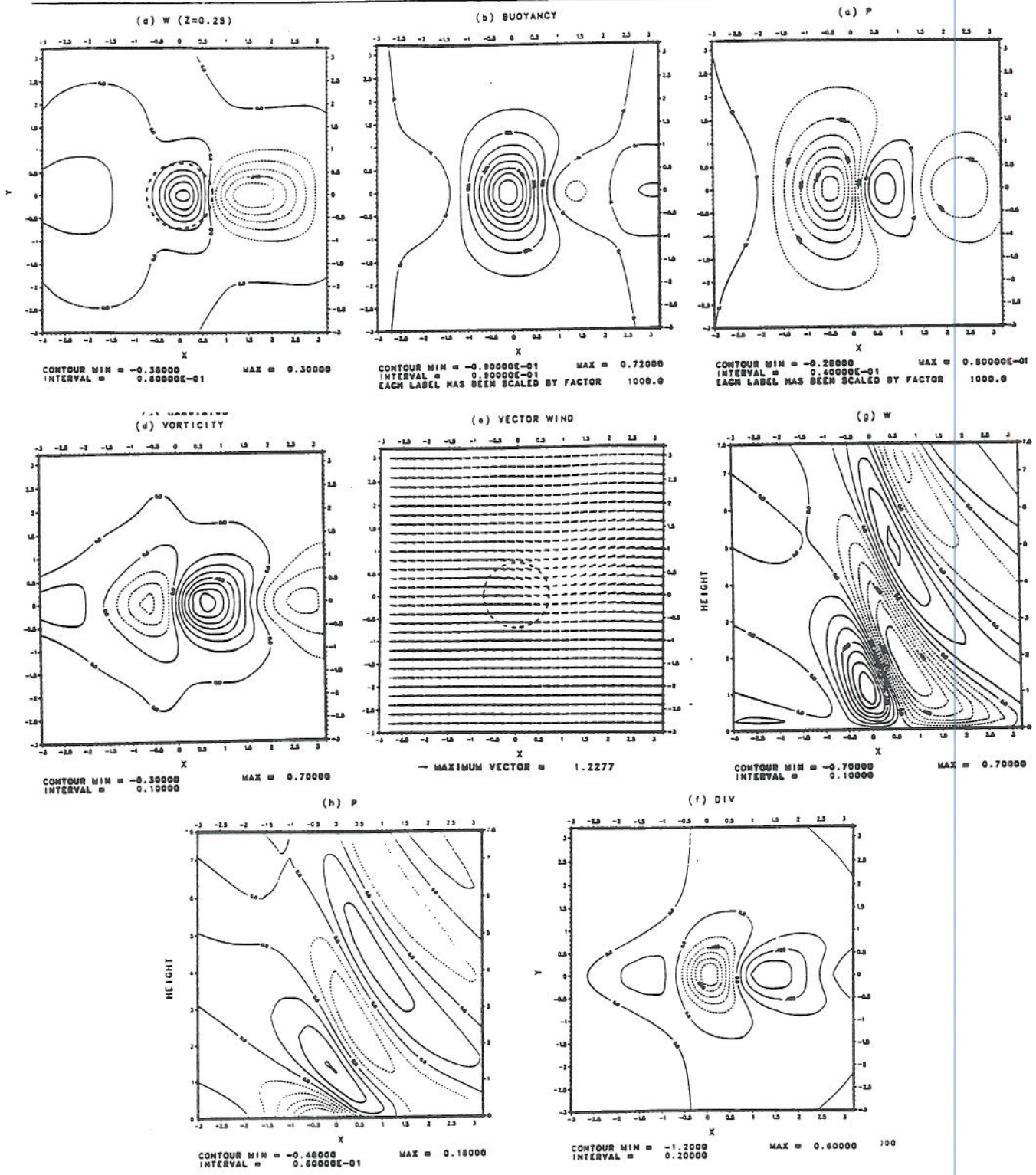

Fig. 44: Same as Fig. 43 except with inertial effects included. The parameters used are: T_0=1.5, b=1, R_0=1, and γ=1. Solutions can be found in Eqs. (6.28)-(6.35). (From Lin, 1989a)

of the vertical velocity is more asymmetric in the basic wind direction than that in the quasi-geostrophic case. The buoyancy field (Fig. 44b) is similar to that of the quasi-geostrophic case, except there exists a region of high buoyancy (less dense) air far downstream. The major region of high buoyancy near the center of the warm region is mainly produced by the diabatic heating and cooling. The indirect effect on the buoyancy due to vertical motion (Eq. (6.11)) is not pronounced at such a low level because the vertical velocity is weak near the surface.

The perturbation pressure pattern (Fig.44c) is no longer similar to the perturbation buoyancy pattern as that of the quasi-geostrophic case. This is mainly caused by the vertical propagation of the thermally induced inertia-gravity waves. In fact, the pressure field is almost out of phase with the buoyancy field. The V-shaped (or U-shaped as used in Smith, 1980) pattern of the perturbation pressure, also pronounced in other fields, is an indication of the upward propagation of energy as shown in a nonrotational mountain wave problem (Smith, 1980) and in a nonrotational diabatic heating problem (Lin, 1986a; Lin and Li, 1988). The group velocity calculation of Smith can be extended to include the Coriolis force, which gives the concentrated region of the wave energy

$$y^2 = \left[\frac{z\, l^2(R_o^2k^2-1)^{1/2}}{k(R_o^2l^2-1)(k^2+l^2)^{1/2}}\right] x \quad , \qquad \text{for } R_o^2k^2 > 1 \tag{6.36}$$

With no rotation, the above equation reduces to the formula derived by Smith. With the rotational effect included, the wave energy is still concentrated near the parabola described by the above equation. However, the latus rectum becomes larger compared to the nonrotational case. In addition, the above equation indicates that only the wave part of the disturbance contributes to the upward propagation of the energy. Therefore the V-shape is less pronounced for a flow with a smaller Rossby number. Further evidence for upward propagation of the wave energy is the upstream tilt of the disturbance as shown in the cross sections at y=0 (Fig. 44g and h). The region of maximum and minimum perturbations are shifted farther downstream with height, which indicates that the wave energy is both propagated upward and advected downstream. The vorticity field indicates that there exists a negative vorticity center just upstream of the warm region center followed by a strong positive vorticity center and a negative vorticity center far downstream (Fig. 44d). The significant difference from the quasi-geostrophic case is that the positive (negative) vorticity is associated with the high (low) pressure, and not the low (high) pressure. The positive vorticity is no longer in phase with the low because the vertical velocity term is as important as the pressure term in Eq. (6.34) for a flow with a larger Rossby number. This distinction has also been made in a study of a low-Froude number flow over a mesoscale mountain, such as the Central Mountain Range of Taiwan, by Lin et al. (1992). In their case, the Taiwan mesolow does not coincide with the mesovortex. The mesolow is located on the southeast slope of the mountain, while the mesovortices are drifting downstream with the basic wind.

Due to the weaker rotational effect, the vector wind does not deflect as strongly as for the quasi-geostrophic case. However, the cyclonic flow around the region of positive vorticity, not the low pressure, is still evident in this case (Fig. 44e). The divergence field is related to the vertical velocity field by Eq.(6.35) (Fig. 44f). A region of convergence near the center of the warm region is accompanied by

two regions of divergence upstream and downstream. Fig. 44g and h shows the cross sections of the vertical velocity and perturbation pressure along y=0. The major difference from the quasi-geostrophic case is that the phase tilts upstream with height. The perturbation pressure field is in phase with the vertical velocity overall, which indicates that the wave energy is propagated upward because the vertical energy flux, $\int p'w'dx$, is positive (Eliassen and Palm, 1960; Jones, 1967).

With the Ekman friction included in the quasi-geostrophic flow, there are three significant features of the resulting disturbance: (i) an upstream-downstream asymmetry, (ii) an upstream phase tilt in the lower layer, and (iii) weakening of the positive vorticity and the low (Lin, 1989a). The upstream-downstream asymmetry is similar to that of Buzzi and Tibaldi (1977) for a quasi-geostrophic flow over a mountain. The low-level upstream phase tilt is consistent with that of Smagorinsky (1953) who investigated the response of a quasi-geostrophic flow over a diabatic source with β effects and baroclinicity included. These two phenomena are explained by the following argument. At z=0, the maximum positive vorticity is located at the warm region center as shown in Fig. 43. According to the lower boundary condition, Eq.(6.13), associated with the Ekman friction, the maximum upward motion will be shifted from the upstream in the interior fluid to the warm region center at the top of Ekman layer (z=0). Thus, there exists an upstream phase tilt with height in the lower layer. The disturbance associated with the upward motion is then advected by the basic wind, which gives the asymmetric pattern of the vertical velocity.

6.2 Baroclinic Flow

The development of this theory of coastal cyclogenesis is analogous to the development of the theory of lee cyclogenesis proposed by Smith (1984, 1986). Both quasi-geostrophic and semigeostrophic flow over a low-level diabatic heat source have been investigated by Lin (1989b, 1990a) and will be reviewed below.

For an inviscid Boussinesq fluid on an f-plane with constant basic state stratification, the linearized quasi-geostrophic potential vorticity equation and the thermodynamic equation applied at the surface can be written (e.g., see Smith, 1984; Bannon, 1986)

$$\left(\frac{\partial}{\partial t}+U\frac{\partial}{\partial x}+V\frac{\partial}{\partial y}\right)\left(\nabla_H^2 p'+\frac{f^2}{N^2}p'_{zz}\right)=\left(\frac{g\rho_o f^2}{c_pT_oN^2}\right)q'_z \tag{6.37}$$

$$\left(\frac{\partial}{\partial t}+U\frac{\partial}{\partial x}+V\frac{\partial}{\partial y}\right)\theta'+u'_g\Theta_x+v'_g\Theta_y+w'\Theta_z=\left(\frac{\theta_o}{c_pT_o}\right)q' \tag{6.38}$$

where subscripts denote partial differentiation. With the hydrostatic, geostrophic wind and thermal wind equations,

$$\theta'=(\theta_o/g\rho_o)\,p'_z, \tag{6.39}$$

$$u'_g=(-1/f\rho_o)\,p'_y;\quad v'_g=(1/f\rho_o)\,p'_x, \tag{6.40}$$

$$U_z=(-g/f\theta_o)\,\Theta_y;\quad V_z=(g/f\theta_o)\,\Theta_x, \tag{6.41}$$

Eq. (6.38) becomes

$$\left(\frac{\partial}{\partial t}+U\frac{\partial}{\partial x}+V\frac{\partial}{\partial y}\right)p'_z-(U_zp'_x+V_zp'_y)+\rho_oN^2w'=\left(\frac{g\rho_o}{c_pT_o}\right)q' \quad \text{at } z=0. \tag{6.42}$$

The baroclinic waves associated with the system of Eqs. (6.37) and (6.42) are dispersive waves with real frequencies (Smith, 1984), which can propagate along the surface of the earth in the presence of a horizontal temperature gradient.

The deformation depth or Rossby depth of the flow, H_o=fL/N, has a value of about 10 km for a flow with f=10^{-4} s^{-1}, L (horizontal scale) = 1000 km, and N=10^{-2} s^{-1}. Compared with the deformation depth, the thickness of the diabatic heating (~1km) is very small. In this way, we may assume that there exists no interior thermal forcing as a first approximation. Using the shallow heating assumption, Eq. (6.37) reduces to the homogeneous form,

$$\nabla_H^2 p' + \left(\frac{f}{N}\right)^2 p'_{zz} = 0 \qquad (6.43)$$

In deriving the above equation, we have assumed that there exists no initial potential vorticity anomaly. Making the Fourier transform of the above equation and applying the upper boundary condition, which requires the solution to be bounded at infinity, and the lower boundary condition, which requires w=0 at z=0 for a flow over a flat surface, we obtain

$$\hat{p}_t + \left[ik\left(U_o+\frac{fU_z}{N|K|}\right)+il\left(V_o+\frac{fV_z}{N|K|}\right)\right]\hat{p} = \left(\frac{-g\rho_o f}{c_p T_o N|K|}\right)\hat{q}, \qquad (6.44)$$

where U_o and V_o are the surface wind speeds in the x and y directions, respectively. The vertical shears, U_z and V_z, are assumed to be constant.

The above equation is similar to Eq. (4.1) of Smith (1984) except for the forcing term. Similar to the uniform flow case (see Sec. 6.1), the heating rate may be approximated by

$$q'(x,y) = c_p\left(U_o\frac{\partial}{\partial x} + V_o\frac{\partial}{\partial y}\right) T'(x,y) \qquad (6.45)$$

Making the Fourier transform of the above equation and a straightforward manipulation of Eq. (4.1) of Smith (1984) and Eq. (6.44), we obtain a relationship between the orographic forcing and the thermal forcing, namely,

$$h_m(x,y) = \left(\frac{-g}{T_o N^2}\right) T'(x,y), \qquad (6.46)$$

where $h_m(x,y)$ is the shape of the mountain. The above equation means that the response of a quasi-geostrophic flow over a stationary cold (warm) region is equivalent to that over a mountain (valley) if the forcings are of the same shape. According to the above equation, a cold region with potential temperature anomaly of 5.3 K corresponds to a mountain with height of 2 km if T_o=260 K and N=0.01 s^{-1}. This analogy has also been illustrated by Smith (1979, Fig. 15) in which an anticyclonic circulation can be produced by a quasi-geostrophic flow over either a mountain or a cold dome.

The solution of Eq. (6.44) can be found by assuming that there exists no pressure perturbation initially,

$$\hat{p}(k,l,z,t) = \left(\frac{-g\rho_o f}{c_p T_o N|K|}\right)\frac{\hat{q}(k,l)\,(1-e^{-Bt})e^{-N|K|z/f}}{B}, \qquad (6.47)$$

where

$$B \equiv ik\left(U_o+\frac{fU_z}{N|K|}\right) + il\left(V_o+\frac{fV_z}{N|K|}\right). \qquad (6.48)$$

The perturbation pressure in the physical domain is then recovered by the inverse Fourier transform. Eq. (6.47) describes the formation of a baroclinic cyclone if there exists a level at which the basic wind reverses direction as will be discussed later. This is similar to the lee cyclogenesis problem as studied in Smith(1984, 1986). We thus propose this mechanism as a possible prototype of East Coast cyclogenesis. The problem is also similar to the Eady model (Eady, 1949) except that the rigid lid assumption is removed. In this way, the baroclinic instability of the Eady type is avoided (e.g., Pedlosky, 1982).

a. Quasi-geostrophic baroclinic wave generation by two-dimensional diabatic heating

For a two-dimensional quasi-geostrophic flow with diabatic heating, Eq. (6.47) reduces to

$$p'(x,z,t) = \left(\frac{-g\rho_o f}{c_p T_o N}\right) \int_{-\infty}^{\infty} \frac{\hat{q}(k)\,(1-e^{-Bt})e^{-N|k|z/f}}{|k|B} e^{ikx} dk \tag{6.49}$$

where

$$B = ik(U_o + H_o U_z);\ H_o = f/N|k| \tag{6.50}$$

As discussed in Smith (1984), the integral in Eq. (6.49) will go to zero (p-->0) as |x|-->∞ due to the rapid oscillation of the exp(ikx) term if the integrand is well behaved according to the Riemann-Lebesque lemma (Lighthill, 1970). This implies that the disturbance will remain locally in the vicinity of the diabatic heat source/sink. The baroclinic waves can only be generated if the denominator of the integrand vanishes for some value of k. This is possible if U_o and U_z have opposite signs, i.e. if there exists a back-sheared basic flow and a wind reversal level ($|k^*| = f/NH^* = -fU_z/NU_o$). An asymptotic solution for large x and t, similar to that of Smith (1986), can be obtained, which describes a train of baroclinic waves extending from the center of the diabatic heating to the moving point $x=U_o t$.

A bell-shaped heat source/sink in the x direction with a horizontal scale of b, such as that of Eq. (4.3) can be used. A Fast Fourier Transform (FFT) algorithm is then employed to obtain the solution in physical space.

Figure 45 shows an example of a baroclinic quasi-geostrophic flow over a diabatic cooling with a cooling rate of -0.24 J(kg-s)$^{-1}$ and a half-width of 75 km. The basic wind is assumed to be of the form U(z)=(-10+ 0.005z) ms^{-1}. This gives a wind reversal level of 2 km. The grid interval and the number of grid points in the x direction used in the calculation are 30 km and 128, respectively. After 6 hr (Fig. 45a), there exists a region of perturbation high pressure near the center of diabatic cooling (x=0). The high is associated hydrostatically with cold air near the cooling center. On the downstream side (x<0), there exists a wider region of weak low-

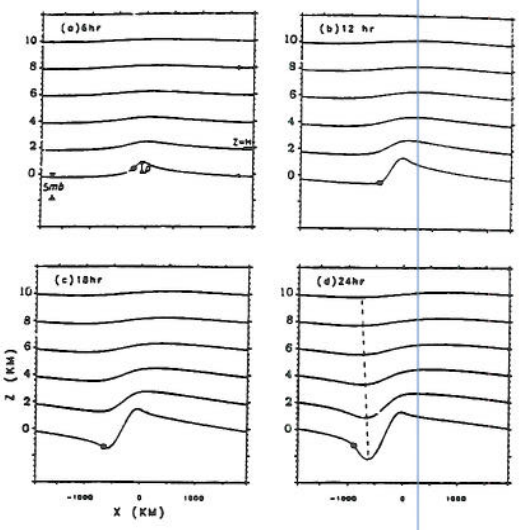

Fig. 45: Two-dimensional baroclinic waves forced by diabatic cooling with a cooling rate of -0.24 J (kg-s)$^{-1}$ and half-width of 75 km. The solution is given by Eq. (6.49) with U(z)=(-10+0.005z) ms^{-1}. Other parameters are: f=10^{-4} s^{-1}, N=10^{-2} s^{-1}, T_o=260 K, and ρ_o=1 kg m^{-3}. Six levels and four time steps of perturbation pressures are shown: (a) 6 h, (b) 12 h, (c) 18 h, and (d) 24 h. The wind reversal level is located at 2 km (labeled by z=H). The location of an air parcel, originating at x=0 and moving with the group velocity ($c_g=U_o$=-10 ms^{-1}) is indicated by a dot at each time step. The arrows in (a) illustrate the direction of the basic wind. The dashed line in (d) is a constant phase line. (From Lin, 1989b)

pressure perturbation. The disturbance decays exponentially with height as indicated by Eq. (6.49). After 12 hr (Fig. 45b), the perturbation high pressure strengthens to a value of about 3.4 mb, while the perturbation low pressure deepens gently to a value of about -1.5 mb. After 18 hr (Fig. 45c), the high pressure deepens to about 3.6 mb, while the low pressure increases to about -3.8 mb. After 24 hr (Fig. 45d), the high pressure weakens to about 3.2 mb, while the low pressure keeps strengthening to a value of -5.6 mb. The upshear vertical tilt of the trough is evidence of the baroclinic wave generated by the diabatic heating. This allows the heat flux to be transported northward meridionally (in the positive y direction) (e.g., see Gill, 1982). The phase line of the trough becomes more vertical at later stage (not shown). Once the available potential energy (APE) stored in the basic baroclinic current has been transferred to the forced baroclinic waves, the phase line will become vertical. For the present case with H=2 km (wind reversal level), the theory predicts a reasonable wavelength of 1250 km ($\lambda=2\pi/k^*=2\pi NH/f$) of the baroclinic wave with a dipolar structure.

Figure 46 shows the time evolution of the absolute minimum and maximum surface perturbation pressures for the case of Fig. 45. The perturbation high pressure grows rather rapidly in the early stage, reaches its maximum of 3.65 mb at 17 hr, and then decays gradually afterwards. The perturbation low pressure develops rather slowly in the first 12 hr, then deepens much more rapidly at later stage. The rapid development of the perturbation low pressure after 12 hr can be explained by a group velocity argument. The group velocity of the baroclinic wave (Smith, 1984, 1986) is

$$c_g = U(H) - \frac{f}{N|k|^3}(k\cdot U_z)\,k, \qquad (6.51)$$

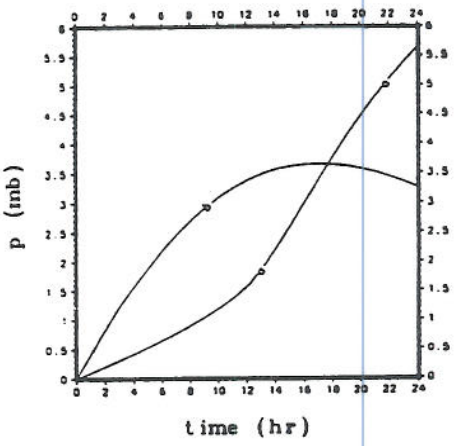

Fig. 46: Time evolution of absolute minimum (a) and maximum (b) surface perturbation pressures for the case of Fig. 45.

where H=f/N|k| and $U(z)=U_0+U_z z$. The above equation reduces to $c_{gz}=U_0$ for a two-dimensional wave (Smith, 1984). As indicated in Eq. (6.45), a moving airstream over the diabatic cooling, $q'(x)=Q_0/[1+(x/b)^2]$, corresponds to that over a cold region extending from x=0 to $-\infty$, $T'(x)=(Q_0 b/c_p U_0)\tan^{-1}(x/b)$. This is analogous to an airflow over a flat plain from a plateau, according to Eq. (6.46). Therefore, the fluid is trying to form a high in the vicinity of the cooling center (x=0) and a first trough downstream (x<0). For example, consider an air parcel originating at x=0 near the surface (denoted by a dot in Fig. 45). It will take 12 hr to advect to 432 km (i.e., x=-432 km in the figure) downstream at the group velocity $c_g=U_0=-10$ ms^{-1}, which is about the region of the developing low (Fig. 45b). During the 12 to 24 hr period, the air parcel reaches the region of the developing low. Thus the low deepens much more rapidly at this stage (Figs. 45c and 46). Like the perturbation high pressure near the cooling center, the perturbation low pressure will reach a

minimum and increase its amplitude afterwards since the air parcel originating at x=0 near the surface will pass through the region of the well-developed low. Thus we may conclude that the diabatic heating plays an important role in converting the available potential energy stored in the baroclinic current to the thermally forced baroclinic wave.

To show the importance of the baroclinicity and the existence of the wind-reversal level in the above cyclogenesis mechanism, we perform four similar cases to the one outlined above, except that now the baroclinicity and wind-reversal level do not exist (Fig. 47). For quasi-geostrophic, baroclinic flow over the diabatic heat source with forward shear (i.e., no wind reversal, Figs. 47a and b), the disturbance is much weaker compared with the corresponding cases with wind reversal (Fig. 45). This indicates that forward vertical wind shear tends to suppress the development of the low or high pressure. For quasi-geostrophic, barotropic flow over the diabatic heating (cooling) region, a perturbation low (high) of -5 mb (+5 mb) is produced after 24 hr (Fig. 47c and d). The surface low (high) produced by the diabatic heating (cooling) is located about 400 km downstream of the heating (cooling) center. Notice that a moving airstream over the diabatic heating corresponds to that over a warm region extending from x=0 to -∞, but with the gradient concentrated in the region of the diabatic heating, for Fig. 47c. The low pressure at the surface is produced by the less dense air above the warm region in a barotropic flow as required by the hydrostatic equation. Thus the low pressure forms on the warm side or the downstream side of the diabatic heating center (x=0). The results are consistent with the quasi-geostrophic flow over a warm region as discussed earlier in Section 6.1. The response is quite different from the low-high couplet produced by diabatic heating in a backsheared baroclinic flow.

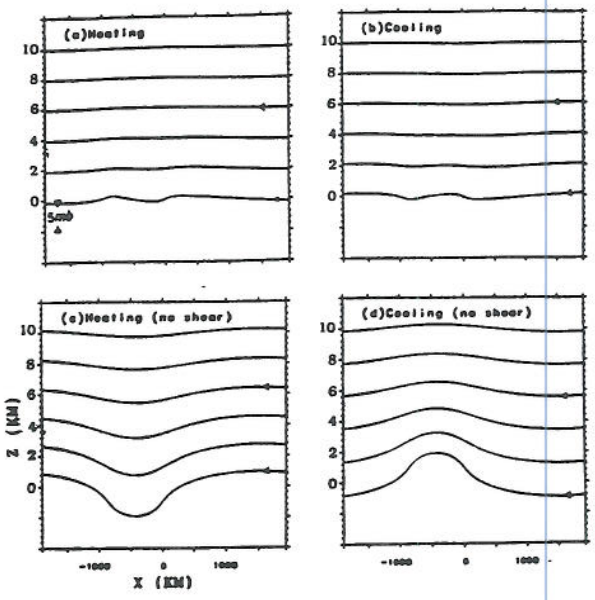

Fig. 47: Six levels of perturbation pressures after 24 h are shown for four cases: (a) Q_o=0.24 J (kg-s)$^{-1}$, U(z)=(-10-0.005z) ms^{-1} (forward shear with heating), (b) same as (a) except with Q_o=-0.24 J (kg-s)$^{-1}$ (forward shear with cooling), (c) Q_o=0.24 J (kg-s)$^{-1}$ (no shear with heating), and (d) same as (c) except with Q_o=-0.24 J (kg-s)$^{-1}$ (no shear with cooling). The heating function is same as that prescribed in Fig. 45.

b. Three-Dimensional Response

Some interesting discussions (Bannon, 1990; Lin, 1990b) have been brought up after the publication of the above proposed cyclogenesis mechanism by Lin (1989b). The major comments of Bannon on Lin's work are: (a) the forcing scale is too small to use the quasi-geostrophic approximation, and (b) the vertical distribution of the surface heating should be included. It is discussed in

Lin's reply (1990b) to (a) that the heating scale should be considered to be larger than its half-width and that the cyclone scale is not directly proportional to the forcing scale in a transient flow, unlike the steady state flow over a mountain. In addition, the quasi-geostrophic approximation is improved in a subsequent paper (Lin, 1990a) using the geostrophic momentum approximation in a semigeostrophic model. For the second comment (b), it is shown by Lin (1990b) that the contribution of the vertical distribution of the surface heating does not alter the low to be a high as claimed in Bannon (1990). In the following, we will show some recent results of a continuously stratified baroclinic flow over a vertically distributed heat source.

Using the geostrophic momentum approximation (Eliassen, 1962; Hoskins, 1975), the nonlinear ageostrophic advection of the geostrophic wind can be included in the model. The governing equaitons in the geostrophic space may be written

$$\left[\frac{\partial}{\partial T}+\left(U-\frac{1}{\rho_o f}\Pi'_Y\right)\frac{\partial}{\partial X}+\left(V+\frac{1}{\rho_o f}\Pi'_X\right)\frac{\partial}{\partial Y}\right]Q_g = \left(\frac{g\rho_o f^2}{c_p T_o N^2}\right)q'_Z \tag{6.52}$$

$$\Pi'_{zt}+\left(U_o-\frac{1}{\rho_o f}\Pi'_y\right)\Pi'_{zx}+\left(V_o+\frac{1}{\rho_o f}\Pi'_x\right)\Pi'_{zy}-U_z\Pi'_x -V_z\Pi'_y+\rho_o N^2 w'=\left(\frac{g\rho_o}{c_p T_o}\right)q' \quad \text{at } Z=0, Z_T \tag{6.53}$$

where

$$Q_g = \nabla_H^2\Pi' + \frac{f^2}{N^2}\Pi'_{ZZ}, \tag{6.54a}$$

$$X = x + \frac{v_g}{f}, \tag{6.54b}$$

$$Y = y - \frac{u_g}{f}, \tag{6.54c}$$

$$Z = z, \tag{6.54d}$$

$$T = t, \tag{6.54e}$$

$$\Pi = p + \frac{\rho_o}{2}(u_g^2 + v_g^2). \tag{6.54f}$$

The potential vorticity is then equal to $Q_g/\rho_o f$. Similar to that in Lin (1990a), the pressure in the geostrophic space is separated into a basic part and a disturbance part, i.e. $\Pi(T,X,Y,Z) = \Pi(Z)+\Pi'(T,X,Y,Z)$. The basic part is assumed to satisfy the hydrostatic balance,

$$\frac{1}{\rho_o}\frac{\partial \Pi}{\partial Z} = \frac{g\Theta}{\theta_o}. \tag{6.55}$$

The lower boundary condition with the mountain and Ekman friction included may be written as

$$w'(T,X,Y) = \left[\frac{\partial}{\partial T}+(U_o+u_g)\frac{\partial}{\partial X}+(V_o+v_g)\frac{\partial}{\partial Y}\right]\cdot h_m(T,X,Y) + \frac{\sqrt{\nu/2f}}{\rho_o f}\nabla_H^2\Pi'(T,X,Y) \quad \text{at } Z=0$$

and the upper boundary condition at the imposed rigid lid is

$$w'(T,X,Y) = 0 \quad \text{at } Z=Z_T \tag{6.56}$$

In the above equation, we have implemented a simple Ekman layer boundary condition as described earlier in Section 6.2. The Ekman number corresponds to ν/fH_o^2 where H_o is a height scale. We then substitute Eq. (6.56) into Eq. (6.53) for the lower boundary condition. The system of Eqs. (6.52) and (6.53) can be solved numerically by the leapfrog and the second-order center-difference schemes applied to the time and space derivatives, respectively. The pressure perturbation in the geostrophic space Π' can be solved from Eq.(6.54a) in the Fourier space and transformed back to the geostrophic space numerically by an FFT algorithm. The variables in the physical space are then recovered by applying the inverse geostrophic transformation based on Eq.

(6.54b-f). In the following, we have used the following numerical parameters: Δt=10 min, $\Delta x=\Delta y$=60 km. The total grid numbers are 64 in both x and y directions. As mentioned earlier, a bounded upper boundary condition is applied at z=10 km. A periodic lateral boundary condition is assumed implicitly by the use of a FFT algorithm.

To check the model, we perform a simulation of baroclinic flow over a bell-shaped mountain. The mountain shape is assumed to be

$$h_m(x,y) = \frac{h_o}{[x^2/a_x^2 + y^2/a_y^2+1]^{3/2}}, \tag{6.57}$$

where a_x and a_y are the horizontal scales of the

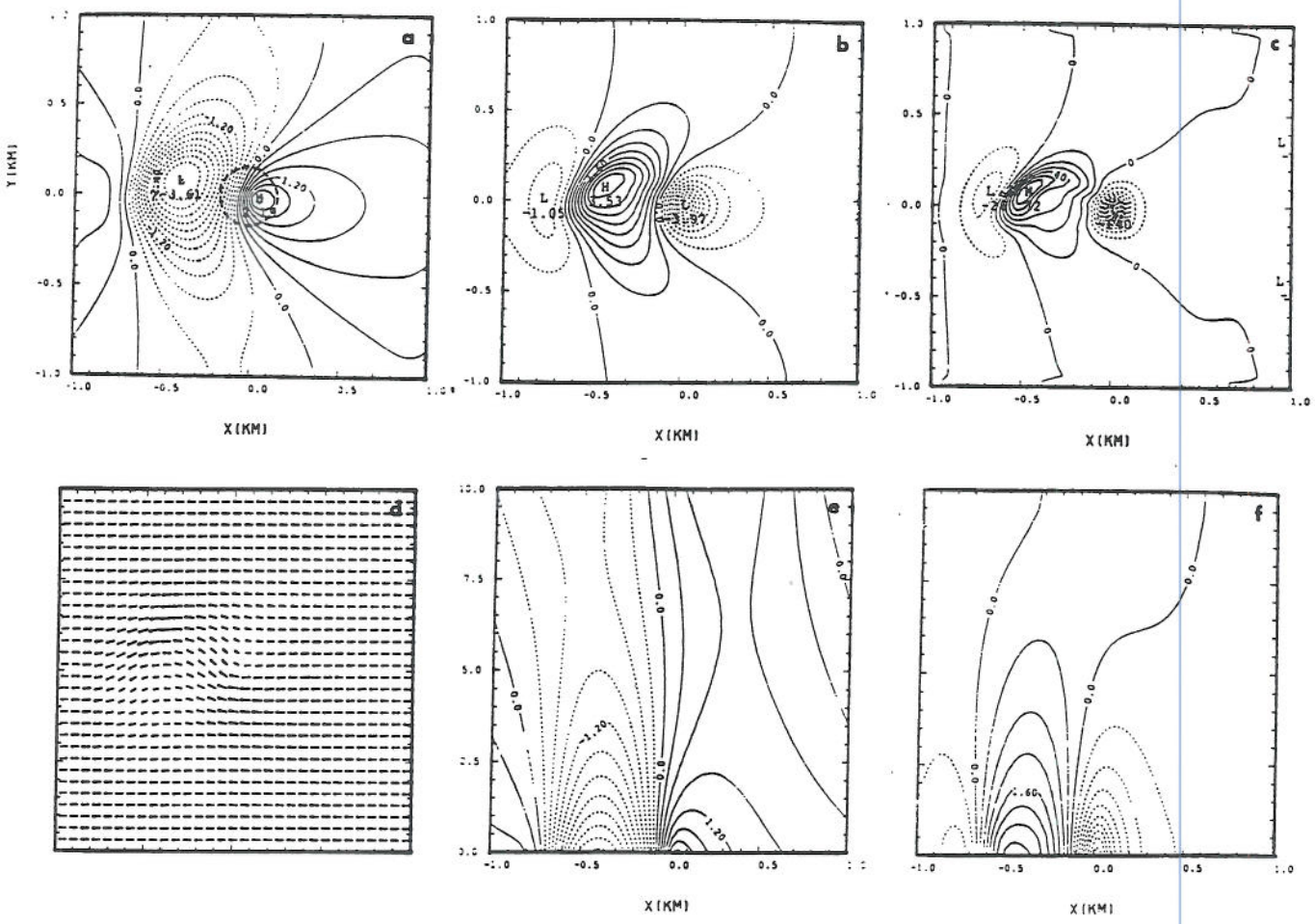

Fig. 48: Inviscid semi-geostrophic continuously stratified baroclinic flow over a bell-shaped mountain with h_o=1.5 km and $a_x=a_y$=250 km. The basic wind is U(z)=(-15+0.004z) ms^{-1} and V(z)=0 ms^{-1}, which blows from east at the surface and reverses its direction at z=3.75 km. Other parameters are: f=10^{-4} s^{-1}, N=0.01 s^{-1}, T_o=260 K, and ρ_o=1 kg m^{-3}. The dashed curve in (a) denotes the terrain contour of 360 m. Four horizontal fields at the surface after 24 h are shown: (a) perturbation pressure, (b) perturbation potential temperature, (c) geostrophic relative vorticity, and (d) vector wind. Vertical cross sections of perturbation pressure and potential temperature along y=0 are shown in (e) and (f), respectively.

mountain in the x and y directions, respectively. The mountain height (h_o) and the horizontal scale ($a_x = a_y$ in this case) of the orography are assumed to be 1.5 km and 250 km, respectively. The basic wind is assumed to be U(z)=(-15+0.004z) ms^{-1} and V(z)=0 ms^{-1}, which blows from east at the surface and reverses its direction at z=3.75 km. The Coriolis parameter is assumed to be 10^{-4} s^{-1}. This case is identical to that of Chen and Smith (1987) except that the basic wind is incident from the east-west direction instead of the north-south direction. Fig. 48 shows the perturbation pressure, perturbation potential temperature, geostrophic vorticity, geostrophic vector wind fields at the surface and cross sections of perturbation pressure and perturbation potential temperature along y=0 after 24 h. The basic features of the semigeostrophic model results are similar to the theoretical results of Smith (1984, 1986) and Chen and Smith (1987) and the nonlinear primitive equation model results of Lin and Perkey (1989). In the vicinity of the mountain top, an anticyclonic flow (Fig. 48d) develops, which is associated with the mountain-induced high pressure (Fig. 48a). The maximum perturbation pressure is 2.2 mb. The mountain high is formed by the subgeostrophic flow of fluid particles approaching the mountain. Fluid particles are deflected slightly to the left upstream of the mountain if one faces downstream. This anticyclonic circulation is also shown in the geostrophic perturbation vorticity field (Fig. 48c). A pool of relatively cold air is associated with this mountain high (Fig. 48b). The perturbation temperature has a minimum of -4.0 K. The low, which has been advected by the mountain high, is formed in the northwest corner to the lee of the mountain (Fig. 48a). The minimum value of the perturbation pressure is -3.6 K. A similar pattern of positive perturbation temperature (warming) (Fig. 48b) is associated with the low. The perturbation temperature reaches a maximum value of 3.5 K. Notice that this pool of warm air is a combined effect of warm advection and downslope adiabatic warming. The cross sections of perturbation pressure and potential temperature (Fig. 48e and f) indicate that the forced baroclinic wave is shallow. Unlike the case of Lin and Perkey (1989), the blocking effect is not pronounced in this case. This is due to the combined effect of a smaller mountain used and the neglect of the nonlinear ageostrophic advection of the ageostrophic wind.

Fig. 49 shows the perturbation pressure, perturbation potential temperature, geostrophic vorticity, and geostrophic vector wind fields at the surface and cross sections of perturbation pressure and perturbation potential temperature along y=0 after 24 h of a continuously stratified baroclinic flow over a bell-shaped heat source with circular contours. The diabatic heating function is prescribed by

$$q'(x,y) = \frac{Q_o}{[x^2/b_x^2 + y^2/b_y^2+1]^{3/2}}, \qquad (6.58)$$

where b_x and b_y are the horizontal scales of the heat source in the x and y directions, respectively. The maximum heating rate (Q_o) and the horizontal scale ($b_x = b_y$ in this case) of the heat source are assumed to be 0.24 J/kg-s and 150 km, respectively. The heating decreases with height exponentially with an e-folding value of 1.5 km. The basic wind is assumed to be U(z)=(-10+0.005z) ms^{-1} and V(z)=0 ms^{-1}, which blows from the east at the surface and reverses its direction at z=2 km. The Rossby number associated with this flow is about 0.33, which is estimated by $U_o/2fb_x$ with U_o=10 ms^{-1}, f=10^{-4} s^{-1}, and $b_x = b_y$=150 km. Notice that we have used the whole width ($2b_x$) for the horizontal scale of the bell-shaped heat source, instead of the half-

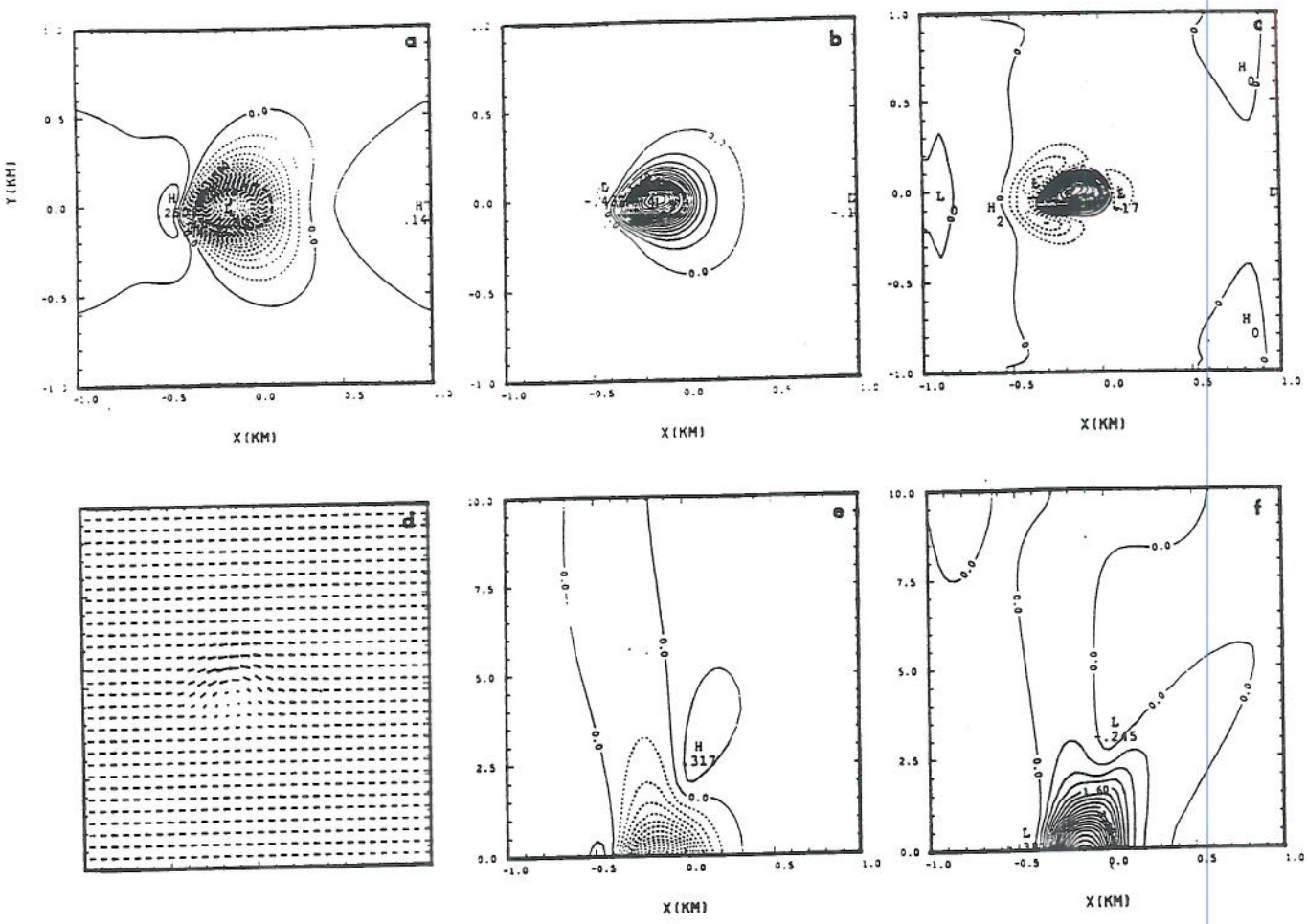

Fig. 49: Same as Fig. 48 except for flow over a bell- shaped heating region with Q_o=0.24 J (kg-s)$^{-1}$ and b_x=b_y=150 km. The heating rate of 0.04 J (kg-s)$^{-1}$ is denoted by the dashed curve in (a). The basic wind is U(z)=(-10+0.005z) ms^{-1} and V(z)=0 ms^{-1}, which blows from east at the surface and reverses its direction at z=2 km. The Rossby number associated with this flow is about 0.33.

width. Hoskins (1975) places a loose upper limit on the Rossby number at R_o=0.5 for use in semi-geostrophic theory. Therefore, the geostrophic momentum approximation may still be adquate for describing the flow in the present case. In response to this isolated diabatic heating, a region of low pressure with a minimum of about -3.19 mb forms in the vicinity of the heating region after 24 hr (Fig. 49a). There exists a much smaller region of relatively weak high pressure downstream of the concentrated heating region. Associated with the perturbation low and high pressures are more compact regions of warm and cold air, respectively (Fig. 49b). This is required by the hydrostatic equation. The low-high couplet associated with the forced baroclinic wave is located in the vicinity of the forcing region. The disturbance remains locally in the vicinity of the thermal forcing because the

thermally forced baroclinic wave has a zero phase speed (Smith, 1984). At the surface, the fluid parcel experiences a cyclonic circulation near the center of the low pressure region where there exists a cell of positive relative vorticity (Fig. 49c). A region of very weak negative vorticity is generated upstream of the heating, while a wider region of stronger negative vorticity is generated downstream of the heating. An inverted trough forms near the heating center (Fig. 49d), which is often observed to form along the Carolina coast in many cyclogenesis events. Both vertical cross sections of pressure and temperature fields (Fig. 49e and f) indicate that the disturbance is confined in a shallow layer. The present results are consistent with those with the assumption of shallow heating (Lin, 1989b, 1990a) except that the magnitude of the disturbance is weaker.

Acknowledgment

The author wishes to express his sincere appreciation to R. B. Smith at Yale University for introducing him to mesoscale dynamics which helped to stimulate the series of work presented in this review. Discussions with R. F. Adler, A. Barcilon, L. F. Bosart, C. Bretherton, W.-D. Chen, D. R. Durran, K. Emanuel, G. M. Heymsfield, R. Hughes, G. S. Janowitz, D. Keyser, D. J. Raymond, R. Rotunno, and W.-Y. Sun among others were very helpful. The author is grateful to R. P. Weglarz and T. A. Wang for reading of the manuscript.

References

Abdullah, A. J., 1955. Bull. Amer. Meteor. Soc., **10**, 511-518.

Adler, R. F., and R. A. Mack, 1986. J. Atmos. Sci., **43**. 1945-1960.

Adler, R. F., D. D. Fenn, and D. A. Moore, 1981. Mon. Wea. Rev., **109**, 194-199.

Anderson, C. E., 1982. Twelveth Conf. on Severe Local Storms, San Antonio, Amer. Meteor. Soc., 493-498.

Anthes, R. A., Y.-H. Kuo, and J. R. Gyakum, 1983. Mon. Wea. Rev., **111**, 1174-1188.

Bannon, P. R., 1986. J. Atmos. Sci., **43**, 2261-2274.

Bannon, P., 1990. J. Atmos. Sci., **47**, 2241-2242.

Barcilon, A., and D. Fitzjarrald, 1985. J. Atmos. Sci., **42**, 58-67.

Barcilon, A., J. C. Jusem, and S. Blumsack, 1980. Geophys. Astrophys. Fluid Dyn., **16**, 19-33.

Bergeron, T., 1968. Met. Inst. Uppsala Univ., Report No. **6**.

Bjerknes, J., 1951. *Compendium of Meteorology*, T. F. Malone, Ed., Amer. Meteor. Soc., 577-598.

Bluestein, H. B., and M. H. Jain, 1985. J. Atmos. Sci., **42**, 1711-1732.

Blumen, W., and R. G. Hendl, 1969. J. Atmos. Sci., **26**, 210-217.

Booker, J. R., and F. P. Bretherton, 1967. J. Fluid Mech., **27**, 513-539.

Bosart, L. F., and J. P. Cussen, 1973. Mon. Wea. Rev., **101**, 446-454.

Bosart, L. F., 1981. Mon. Wea. Rev., **109**, 1542-1566.

Bosart, L. F., 1988. GALE/CASP Workshop Reports, 75-93.

Braham, R. R., and M. J. Dungey, 1978. J. Appl. Meteor., **17**, 644-654.

Bretherton, C., 1988. J. Atmos. Sci., **45**, 81-93.

Bretherton, F. P., 1966. Quart. J. Roy. Meteor. Soc., **92**, 466-480.

Bretherton, F. P., 1969. J. Atmos. Sci., **45**, 81-93.

Browning, K. A., C. W. Pardoe, and F. F. Hill, 1974 Quart. J. Roy. Meteor. Soc., **100**, 309-

330.

Browning, K. A., 1980. GARP Publication Series #23, WMO, Geneva.

Buzzi, A., and S. Tibaldi, 1977. Quart. J. Roy. Meteor. Soc., **103**, 135-150.

Changnon, S. A., 1981. Met. Monograph., **40**, Amer. Meteor. Soc., 181 pp.

Charney, J. G., and A. Eliassen, 1949. Tellus, **1**, 38-54.

Chen, C., J. W. Rottman, and S. E. Koch, 1992. Fifth Conf. on Meso. Proc., Atlanta, Georgia, pp. 241-245.

Chen, W.-D., and R. B. Smith, 1987. Sixth Extratropical Cyclone Workshop, Monterey, CA.

Christie, D. R., K. J. Muirhead, and A. L. Hales, 1978. J. Atmos. Sci., **35**, 805-825.

Crook, N. A., and M. W. Moncrieff, 1988. J. Atmos. Sci., **45**, 3606-3624.

Chun, H.-Y, and Y.-L. Lin, 1992. Submitted to J. Atmos. Sci.

Davies, H. C., and C. Schar, 1986. Quart. J. Roy. Meteor. Soc., **112**, 711-730.

DeMaria, M., 1985. J. Atmos. Sci., **42**, 1944-1959.

DeSouza, R. L., 1972. Master's thesis, Dept. of Meteor., Florida State Univ., 203 pp.

Durran, D. R., and J. B. Klemp, 1982. J. Atmos. Sci., **39**, 2490-2506.

Eady, E. T., 1949. Tellus, **3**, 36-52.

Eliassen, A., 1962. Geofys. Publ., **24**, 147-160.

Eliassen, A., and E. Palm, 1960. Geofys. Publ., **22**, 1-23.

Emanuel, K., and D. J. Raymond, 1984. *Dynamics of mesoscale weather systems*. J. B. Klemp (ed.), NCAR Summer Colloquium Lecture Notes. 591 pp.

Estoque, M. A., 1962. J. Atmos. Sci., **19**, 244-250.

Ferguson, H. L., 1967. J. Appl. Meteor., **6**, 523-529.

Fraser, A. B., R. Easter and P. Hobbs, 1973. J. Atmos. Sci., **30**, 813-823.

GALE, 1986. T. J. Mercer and C. W. Kreitzberg, Eds., GALE Data Center, Drexel University, Philadelphia.

Garstang, M., P. D. Tyson, and G. D. Emmitt, 1975. Rev. Geophys. Space Phys., **13**, 139-165.

Geisler, J. E., 1981. J. Atmos. Sci., **38**, 1390-1400.

Geisler, J. E., and F. P. Bretherton, 1969. J. Atmos. Sci., **26**, 82-95.

Geisler, J. E., and D. E. Stevens, 1982. Quart. J. Roy. Meteor. Soc., **108**, 87-94.

Gill, A. E., 1980. Quart. J. Roy. Meteor. Soc., **106**, 447-462.

Gill, A. E., 1982. *Atmosphere-Ocean Dynamics*. Int. Geophys. Ser., Vol. 30, Academic Press, 662 pp.

Goldstein, S., 1931. Proc. Roy. Soc. London, **A132**, 524-548.

Gossard, E. E., and W. H. Monk, 1975. *Waves in the Atmosphere*. Elsevier Scientific, 456 pp.

Grimshaw, R., 1981. Phys. Fluids, **24**, 1611-1618.

Grossman, R. L., and D. R. Durran, 1984. Mon. Wea. Rev., **112**, 652-672.

Henz, J. F., 1972. J. Appl. Meteor., **11**, 1284-1292.

Heymsfield, G. M., and R. H. Blackmer, Jr., 1988. J. Atmos. Sci., **116**, 2200-2224.

Heymsfield, G. M., R. H. Blackmer, Jr., and S. Schotz, 1983a. Part I. J. Atmos. Sci., **40**, 1740-1755.

Heymsfield, G. M., G. Szejwach, S. Schotz, and R. H. Blackmer, Jr., 1983b. Part II. J. Atmos.

Sci., 40, 1756-1767.

Heymsfield, G. M., R. Fulton, and J. D. Spinhirne, 1991. J. Atmos. Sci., 119, 436-456.

Hildebrand, F. B., 1976. *Advanced Calculus for Applications*. 2nd ed., Prentice-Hall Inc., 733 pp.

Hjelmfelt, M. R., 1982. J. Appl. Meteor., 31, 1239-1257.

Hobbs, P. V., R. Houze, Jr., and T. Matejka, 1975. J. Atmos. Sci., 32, 1542-1562.

Hoiland, E., 1951. Fifth Prog. Rep., Contract AF19(122)-263. Air Force Cambridge Research Center.

Hoskins, B. J., 1975. J. Atmos. Sci., 32, 233-242.

Hoskins, B. J., and D. J. Karoly, 1981. J. Atmos. Sci., 38, 1179-1196.

House, D. C., 1961. Bull. Amer. Meteor. Soc., 42, 803-816.

Hsu, H.-M., 1987a. J. Atmos. Sci., 44, 186-199.

Hsu, H.-M., 1987b. J. Atmos. Sci., 44, 1019-1040.

Hunt, J. N., R. Palmer, and W. Penney, 1960. Phil. Trans. Roy. Soc., London, A252, 275-315.

Jones, W. L., 1967. J. Fluid Mech., 30, 439-448.

Kaplan, M. L., and D. A. Paine, 1977. Beitr. Phys. Atmos., 50, 321-330.

Klemp, J. B., and D. K. Lilly, 1978. J. Atmos. Sci., 35, 78-107.

Klemp, J. B., and R. B. Wilhelmson, 1978. J. Atmos. Sci., 35, 1070-1096.

Koch, S. E., and P. B. Dorian, 1988. Part III. Mon. Wea. Rev., 116, 2570-2592.

Lamb, H., 1932. *Hydrodynamics*. Dover Publications, 6th Ed., 738pp.

Lau, K. M., and H. Lim, 1984. J. Atmos. Sci., 41, 161-176.

LeBlond, P. H., and L. A. Mysak, 1978. *Waves in the Ocean*. Elsevier Scientific, 602 pp.

Lighthill, M. J., 1970. *Introduction to Fourier Analysis and General Fuctions*. Cambridge University Press, 79pp.

Lilly, D. K., 1979. Ann. Rev. Earth Planet. Sci., 7, 117-161.

Lim, H., and C. P. Chang, 1983. J. Atmos. Sci., 40, 1897-1915.

Lin, C. A., and R. E. Stewart, 1991. Adv. Geophys., 33, B. Saltzman (ed.), Academic Press, NY, 267-305

Lin, C. A., K. K. Szeto, and R. E. Stewart, 1988a. Part I. J. Atmos. Sci., 45, 1629-1641.

Lin, C. A., R. E. Stewart, and K. K. Szeto, 1988b. Part II. J. Atmos. Sci., 45, 1642-1650.

Lin, Y.-L., 1986a. J. Atmos. Sci., 43, 2736-2751.

Lin, Y.-L., 1986b. Pap. Meteor. Res., 9, 19-45.

Lin, Y.-L., 1987. J. Atmos. Sci., 44, 1375-1393.

Lin, Y.-L., 1989a. J. Atmos. Sci., 46, 921-936.

Lin, Y.-L., 1989b. Part I. J. Atmos. Sci., 46, 3015-3036.

Lin, Y.-L., 1990a. Part II. J. Atmos. Sci., 47, 1755-1777.

Lin, Y.-L., 1990b. Part I. J. Atmos. Sci., 47, 2243-2244.

Lin, Y.-L., and H.-Y. Chun, 1991. J. Atmos. Sci., 48, 2476-2491.

Lin, Y.-L., and R. C. Goff, 1988. J. Atmos. Sci., 45, 194-205.

Lin, Y.-L., and D. J. Perkey, 1989. J. Atmos. Sci., 46, 3685-3697.

Lin, Y.-L., and Shiaolin Li, 1988. J. Atmos. Sci., 45, 2987-3002.

Lin, Y.-L., and R. B. Smith, 1986. J. Atmos. Sci., 43, 40-49.

Lin, Y.-L., R. D. Farley, and H. D. Orville, 1983. J. Climate Appl. Meteor., 22, 1065-1092.

Lin, Y.-L., N.-H. Lin, and R. P. Weglarz: 1992. Meteor. Atmos. Phys., in print.

Lindzen, R. S., 1974. J. Atmos. Sci., **31**, 156-179.

Lindzen, R. S., and K.-K. Tung, 1976. Mon. Wea. Rev., **104**, 1602-1617.

Luthi, D., C. Schar, and H. C. Davies, 1989. Contri. Atmos. Phys., **62**, 126-150.

Mahrer, Y., and R. a. Pielke, 1976. Mon. Wea. Rev., **104**, 1392-1402.

Malkus, J. S., and M. E. Stern, 1953. Part. I, J. Meteor., **10**, 30-41.

Malkus, J. S., 1963. J. Appli. Meteor., **2**, 547-556.

Marwitz, J. D., 1972. Part I. J. Appl. Meteor., **11**, 166-179.

Marwitz, J. D., 1980. Part I. J. Appl. Meteor., **19**, 913-926.

Maslowe, S. A., 1986. Ann. Rev. Fluid Mech., **18**, 405-432.

Negri, A. J., 1982. Bull. Amer. Meteor. Soc., **63**, 1151-1159.

Newton, C. W., 1966. Tellus, **18**, 699-712.

Nicholls, M. E., R. A. Pielke and W. R. Cotton, 1991. J. Atmos. Sci., **48**, 1869-1884.

Olfe, D. B., and R. L. Lee, 1971. J. Atmos. Sci., **28**, 1374-1388.

Ogura, Y., and Y.-L. Chen, 1977. J. Atmos. Sci., **34**, 1458-1476.

Ogura, Y., and M.-T. Liou, 1980. J. Atmos. Sci., **37**, 553-567.

Ogura, Y., and M. Yoshizaki, 1988. Mon. Wea. Rev., **45**, 2097-2122.

Orlanski, I., 1975. Bull. Amer. Meteor. Soc., **56**, 527-530.

Orlanski, I., and J. J. Katzfey, 1987. Mon. Wea. Rev., **115**, 2792-2821.

Palm, E., 1953. Astrophys. Norvegica, Vol. V, No. 3, 1-129.

Pecnick, M. J., and J. A. Young, 1984. J. Atmos. Sci., **41**, 1850-1862.

Pedlosky, J., 1982. *Geophysical Fluid Dynamics*. Springer-Verlag, 2nd ed., 624 pp.

Pekeris, C. L., 1948. Part II. Phys. Rev., **73**, 145-154.

Pierrehumbert, R. T., and B. Wyman, 1985. J. Atmos. Sci., **42**, 977-1003.

Queney, P., 1947. Dept. Meteor., Univ. of Chicago, Misc. Report No. 23, 81 pp.

Queney, P., 1954. Sci. Rep. No. 1, Contract AF19(604)-728. Air Force Cambridge Research Center.

Queney, P., G. A. Corby, N. Gerbier, H. Koschmieder, and J. Zierep, 1960. WMO Tech. Note, No. **34**, Ed. Alaka.

Ramage, C. S., 1971. *Monsoon Meteorology*. Academic Press, NY, 296 pp.

Ramakrishnan, K. P., and B. Gopinatha Rao, 1958. Symposium on the Monsoon World, Indian Meteor. Dept.

Raymond, D. J., 1972. J. Atmos. Sci., **29**, 837-843.

Raymond, D. J., 1983. J. Atmos. Sci., **40**, 2561-2572.

Raymond, D. J., 1984. J. Atmos. Sci., **41**, 1946-1958.

Raymond, D. J., 1986n. J. Atmos. Sci., **43**, 1011-1111.

Raymond, D. J., and R. Rotunno, 1989. J. Atmos. Sci., **46**, 2830-2837.

Rhea, J. O., 1966. J. Appl. Meteor., **5**, 58-63.

Robichaud, A., and C. A. Lin, 1989. J. Geophys. Res., **94**, 3413-3426.

Rotunno, R., 1983. J. Atmos. Sci., **40**, 1999-2005.

Rotunno, R., J. B. Klemp, and M. L. Weisman,

1988. J. Atmos. Sci., **45**, 463-485.

Sarker, R. P., 1967. Mon. Wea. Rev., **95**, 673-684.

Schlesinger, R. E., 1980. Part II. J. Atmos. Sci., **37**, 395-420.

Schlesinger, R. E., 1984. J. Atmos. Sci., **41**, 1551-1570.

Schlesinger, R. E., 1988. Part I. J. Atmos. Sci., **45**, 1555-1570.

Scorer, R. S., 1950. Proc. Roy. Soc., London, **A201**, 137-157.

Scorer, R. S., 1954. Quart. J. Roy. Meteor. Soc., **80**, 417-428.

Seitter, K. L., and H.-L. Kuo, 1983. J. Atmos. Sci., **40**, 2831-2854.

Simmons, A. J., 1982. Quart. J. Roy. Meteor. Soc., **108**, 503-534.

Smagorinsky, J., 1953. Quart. J. Roy. Meteor. Soc., 79, 342-366.

Smith, R. C., 1955. Q. J. Roy. Meteor. Soc., **81**, 382-395.

Smith, R. C., 1957. Part II. Quart. J. Roy. Meteor. Soc., **83**, 248-256.

Smith, R. B., 1979. Adv. in Geophys., **21**, B. Saltzman (ed.), Academic Press, NY, 87-230.

Smith, R. B., 1980. Tellus, **32**, 348-364.

Smith, R. B., 1982. Mon. Wea. Rev., **110**, 306-309.

Smith, R. B., 1984. J. Atmos. Sci., **41**, 1159-1168.

Smith, R. B., 1985. Mon. Wea. Rev., **113**, 2176-2177.

Smith, R. B., 1986. J. Atmos. Sci., **43**, 1582-1602.

Smith, R. B., 1989. J. Atmos. Sci., **46**, 3611-3613.

Smith, R. B., and Y.-L. Lin, 1982. Quart. J. Roy. Meteor. Soc., **108**, 353-378.

Smith, R. B., and Y.-L. Lin, 1983. Mountain Meteorology, Eds. E. R. Reiter et al., Sci. Press and Amer. Meteor. Soc., 71-94.

Smolarkiewicz, P. K., and R. Rotunno, 1989. Part I. J. Atmos. Sci., **46**, 1154-1164.

Stobie, J. G., F. Einaudi, and L. W. Uccellini, 1983. J. Atmos. Sci., **40**, 2804-2830.

Spiegel, E. A., and G. Veronis, 1960. Astrophys. J., **131**, 442-447.

Sun, W.-Y. and Y. Ogura, 1979. J. Atmos. Sci., **36**, 235-254.

Taylor, G. I., 1931. Proc. Roy. Soc. London, **A132**, 499-523.

Thorpe, A. J., M. J. Miller, and M. W. Moncrieff, 1980. Quart. J. Roy. Meteor. Soc., **106**, 463-484.

Thorpe, A. J., M. J. Miller, and M. W. Moncrieff, 1982. Quart. J. Roy. Meteor. Soc., **108**, 739-762.

Uccellini, L. W., and S. E. Koch, 1987. Mon. Wea. Rev., **115**, 721-729.

Uccellini, L. W., and P. J. Kocin, 1987. Wea. Forecasting, **1**, 289-308.

Uccellini, L. W., P. J. Kocin, R. A. Peterson, C. H. Wash, and K. F. Brill, 1984. Mon. Wea. Rev., **112**, 31-55.

Wagner, J. A., 1962. Mon. Wea. Rev., **90**, 431-436.

Webster, P. J., 1972. Mon. Wea. Rev., **100**, 518-541.

Weston, V. H., 1962. Can. J. Phys., **40**, 446-452.

Wyss, J., and K. A. Emanuel, 1988. Mon. Wea. Rev., **116**, 790-794.